In recognition of the importance of preserving what has been written, it is a policy of the American Institute of Physics to have books published in the United States printed on acid-free paper.

AIP Press
American Institute of Physics
500 Sunnyside Boulevard
Woodbury, NY 11797-2999

Library of Congress Cataloging-in-Publication Data
Physical properties of polymers handbook / editor, James E. Mark.
p. cm.
Includes bibliographical references and indexes.
ISBN 1-56396-295-0 (book)
ISBN 1-56396-598-4 (CD-ROM)
ISBN 1-56396-599-2 (set)
1. Polymers. I. Mark, James E., 1934–
TA455.P58P475 1996
620.1'92--dc20 95-50256
CIP

10 9 8 7 6 5 4 3 2 1

CHAPTER 34

Conducting Polymers: Electrical Conductivity

R. S. Kohlman, J. Joo[1] and A. J. Epstein[2]

Department of Physics, The Ohio State University, Columbus, OH 43210-1106

34.1	Introduction	453
34.2	Conductivity	455
34.3	Structural Order	458
34.4	Density of States	459
34.5	Temperature Dependent Conductivity and Magnetoresistance	461
34.6	Thermoelectric Power	465
34.7	Microwave Dielectric Constant	465
34.8	Optical Absorption, Transmission, and Reflection	467
34.9	Ultimate Conductivity	472
34.10	Applications	472
34.11	Summary	473
	Acknowledgments	473
	Glossary of Terms	473
	References	475

34.1 INTRODUCTION

For the past 50 years, conventional insulating polymer systems have been increasingly used as substitutes for structural materials such as wood, ceramics, and metals because of their high strength, light weight, ease of chemical modification/customization, and processibility at low temperatures [1]. In 1977, the first electrically conducting organic polymer, doped polyacetylene, was reported [2], spurring interest in "conducting polymers [3]." The common electronic feature of pristine (undoped) conducting polymers is the π-conjugated system which is formed by the overlap of carbon p_z orbitals and alternating carbon-carbon bond lengths [4–6], shown schematically in Fig. 34.1. (In some systems, notably polyaniline, nitrogen p_z orbitals and C_6 rings are also part of the conjugation path.) Fig. 34.2 shows the chemical repeat units of pristine forms of several families of conducting polymers, i.e., *trans*- and *cis*-polyacetylene [$(CH)_x$], poly(1,6-heptadiyne), the leucoemeraldine base (LEB), emeraldine base (EB), and pernigraniline base (PNB) forms of polyaniline (PAN), polypyrrole (PPy), polythiophene (PT), poly(*p*-phenylene) (PPP), poly(*p*-phenylene vinylene) (PPV), polypyridine (PPyr), and poly(*p*-pyridyl vinylene) (PPyV). The electronic ground states of these systems are varied. Undoped *trans*-$(CH)_x$ has a twofold degenerate insulating ground state stabilized by the electron-phonon interaction (Peierls instability) [7] and contributions due to Coulomb repulsion [8–12]. Poly(1,6-heptadiyne) [13] and the pernigraniline oxidation state of PAN [14–16] and their derivatives also have degenerate ground states; that is, single and double bonds (benzenoid and quinoid rings for pernigraniline base polymer) can be interchanged without affecting the ground state energy. The remaining polymers illustrated in Fig. 34.2 and their derivatives have nondegenerate ground states; that is, interchange of single and double bonds leads to electronic structures of different energy [7].

The conductivities of the pristine polymers are transformed from insulating to metallic through the process of doping, with the conductivity increasing as the doping level increases. Both *n*-type (electron donating) and *p*-type (electron accepting) dopants have been utilized to induce an

[1]Current address; Department of Physics, Korea University, Seoul, Korea.
[2]Also Department of Chemistry, The Ohio State University; author to whom correspondence should be addressed.

insulator-metal transition in electronic polymers [2–7]. The doping procedures differ from conventional ion implantation used for three-dimensional semiconductors. The doping process for polymers is carried out electrochemically or by exposing the films to vapors or solutions of the dopant [4]. Unlike substitutional doping, as occurs for conventional semiconductors, in electronic polymers the dopant atoms are positioned interstitially between chains, and donate charge to or accept charge from the polymer backbone [2,4,17]. The polymer backbone and dopant ions form new three-dimensional structures. There is a rich variety in these structures, with differing structures occurring for different dopant levels, different structures for different processing routes, and varying degrees of local order [18–20].

The negative or positive charges initially added to the polymer chain upon doping do not simply begin to fill the rigid conduction or valence bands, immediately causing metallic behavior. The strong coupling between electrons and phonons causes lattice distortions around the doped charge [7]. For the degenerate ground states, charges added to the backbone through doping or photoexcitation are stored in soliton and polaron states [5–7,21–24]. For nondegenerate systems, the charges introduced by low doping or photoexcitation are stored as polarons or bipolarons (PT [25–30], PPy [26,31–34], PPV [35–37], PPP [38–40], and polyaniline [41,42]). Photoexcitation also leads to generation of neutral solitons [43,44] and neutral excitons [44–51]. At heavy doping of *trans*-polyacetylene, a soliton lattice that essentially overlaps the valence and conduction band is proposed to form [52,53]. For nondegenerate polymers, heavier doping to the metallic state results in polarons interacting to form a "polaron lattice" or partly filled energy band [54–56]. Some models suggest equilibrium between polarons and bipolarons [33,37,40].

In contrast to the *n*- and *p*-type doping processes applied to polyacetylene, polypyrrole, polythiophene, leucoemeraldine base, etc., for polyaniline emeraldine base (EB) form, the conductivity varies with proton (H^+ ion) doping level. In the protonation process, there is no addition or removal of electrons to form the conducting state [54]. Fig. 34.3

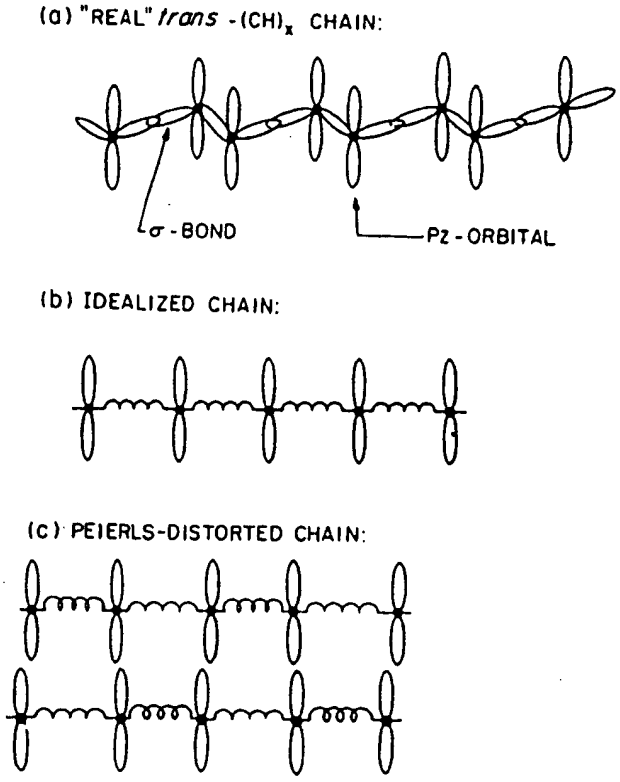

FIGURE 34.1. (a) Schematic view of the carbon backbone of *trans*-polyacetylene chain showing σ-bonds (overlap of sp^3 orbitals of adjacent carbon atoms) and p_z orbitals which form the π and π^* bands that are involved in the electronic properties of the semiconducting and metallic states. (b) An idealization of the chain in *trans*-polyacetylene representing the role of the σ bond as a spring of force constant K. (c) Dimerized ground state reflecting the effects of electron-phonon coupling. Note the two possible phases of the dimerization each of equal energy in this degenerate ground state system. (After J. Orenstein in Ref. 4.)

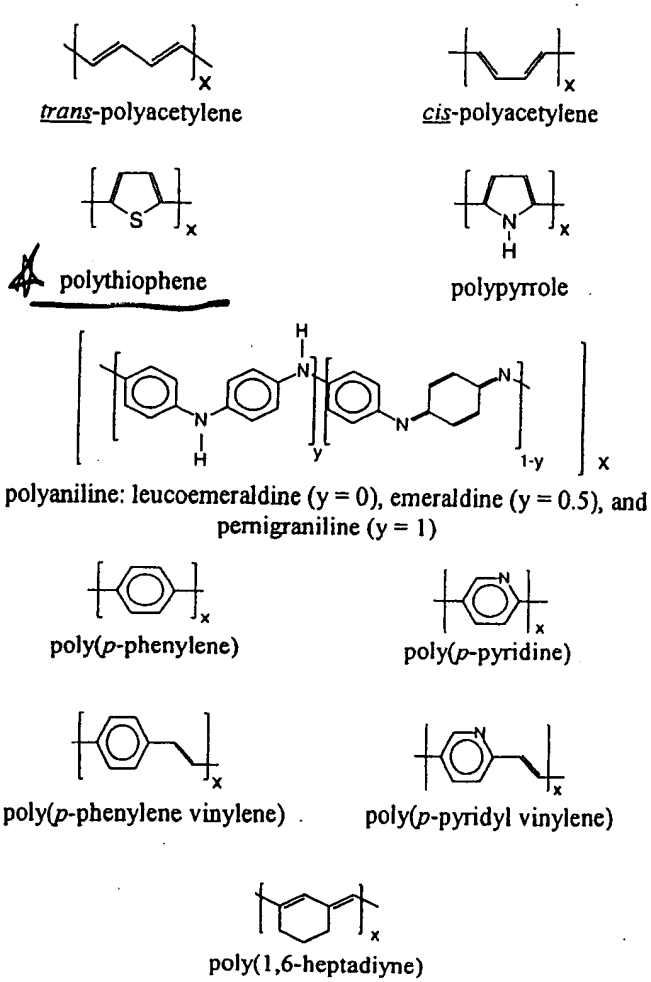

FIGURE 34.2. Repeat units of several electronic polymers.

schematically demonstrates the equivalence of protonic acid doping of emeraldine base and p-doping of leucoemeraldine base to form the conducting emeraldine salt. Similar electronic behavior has been observed for protonic acid doped PAN [54,55,57–60] as for the other nondegenerate ground state systems. Polarons are important at low doping, and, for doping into the metallic state, a polaron lattice forms [54,55,61]. Bipolarons are formed in less ordered regions [62].

Doped polyacetylene has been the prototype system since the initial report of the achievement of a conductivity of $\sigma \sim 100$ S/cm [100 $(\Omega\text{-cm})^{-1}$] upon doping with iodine and other donors and acceptors [2]. Subsequently, $(CH)_x$ was synthesized by alternate routes [63–69] that yielded higher conductivities upon doping. The room temperature dc conductivity (σ_{DC}) for doped films of some of these new materials has been reported to be as high as $\sim 10^5$ S/cm [63,64], rivaling that of traditional metals ($\sigma_{DC} \sim 10^4 - 6\times10^5$ S/cm). Recent advances in the processing of other conducting polymer systems has led to improvements in their σ_{DC}, to the range of $\sim 10^3 - 10^4$ S/cm [3,63–65,70–72], renewing interest in the properties of the polymer metallic state. It is noted that the absolute value of the highest conductivities achieved remains controversial. With these improvements in σ_{DC}, many traditional signatures of an intrinsic metallic nature have become apparent, including negative dielectric constants, a Drude metallic response [73–75], temperature independent Pauli susceptibility [61,62,75–79], and a linear dependence of thermoelectric power on temperature [80,81]. However, the conductivities of even new highly conducting polymers, though comparable to traditional metals at room temperature, generally decrease as the temperature is lowered. Some of the most highly conducting samples remain highly conducting though even in the millikelvin range [70,82]

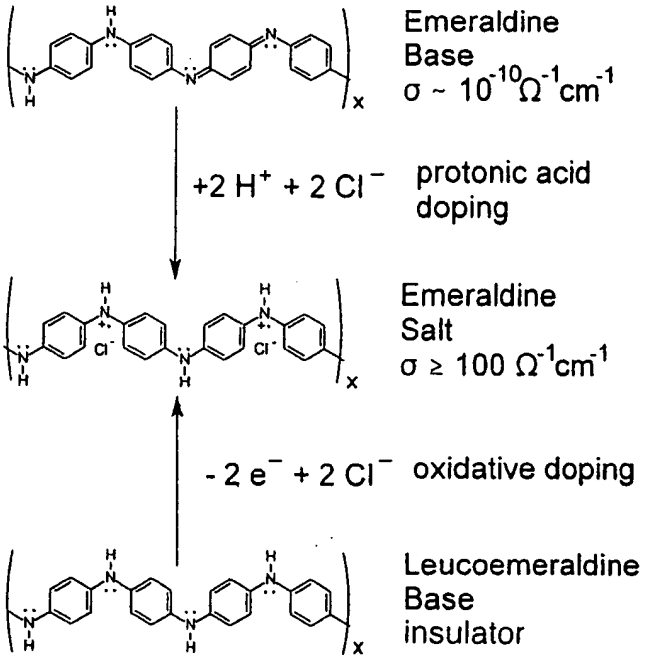

FIGURE 34.3. Illustration of the oxidative doping (p-doping) of leucoemeraldine base and protonic acid doping of emeraldine base, leading to the same final product, emeraldine salt.

Since there is still a great diversity in the properties of materials synthesized by even the same synthetic routes, in presenting properties of these polymers, correlated structural, transport, magnetic, and optical studies of the same materials are emphasized. In this chapter, the intrinsic properties of the metallic state of a broad class of conducting polymers will be reviewed with emphasis on the universality in the observed behaviors. Throughout the article, the correlation of x ray, dc and ac transport, optical, and magnetic measurements will be stressed to demonstrate the relationships where such correlated data is available. On those systems where the correlated results are not available, the available data will be summarized.

The outline for the chapter is as follows. A brief overview of conductivities of various conducting polymers is presented in the section on Conductivity. This section summarizes models for the insulator-metal transition, localization, and metallic conductivity. In the section on Structural Order, the structural results of x ray diffraction studies are introduced. The section on Density of States surveys the metallic density of states of highly conducting polymers. The results of temperature-dependent dc conductivity, thermoelectric power, and microwave dielectric constant are reviewed in the sections on Temperature Dependent Conductivity and Magnetoresistance, Thermoelectric Power, and Microwave Dielectric Constant, respectively. In the section on Optical Absorption, Transmission, and Reflection, the optical properties of the highly conducting state are presented. A discussion of the ultimate conductivity of conducting polymers is given in the section on Ultimate Conductivity, and applications of conducting polymers are introduced in the section on Applications. The last two sections are a summary and a glossary of frequently used terms in the chapter.

34.2 CONDUCTIVITY

34.2.1 Overview of Conductivity of Conducting Polymers

Figure 34.4 presents representative values of the room temperature conductivities reported [17,63–65,71–73,83–98] for the most widely studied doped conducting polymers. Also indicated is the dopant utilized for each value shown. The conductivities of each of these systems increase by more than 10 orders of magnitude upon doping the pristine polymer.

34.2.2 Models of Insulator-Metal Transition

Many efforts have been made to account for the insulator-metal transition that occurs with an increasing doping level in conducting polymers. The richest area of theoretical work concerning the insulator-metal transition is for polyacetylene, which has been studied for the longest time. One of the simplest approaches is to include only the nearest neighbor overlap (leading to a one-dimensional energy band) and the electron-phonon interaction in the starting Hamiltonian [7,21–23]. Within this model, a metallic state is not stable for an isolated one-dimensional chain due to the formation of a Peierls distortion [99] yielding an energy gap at the Fermi level. Negative (n-type) or positive (p-type) doping leads to formation of negatively or positively charged solitons that form completely filled or empty bands [7]. The Su-Schrieffer-Heeger (SSH) Hamiltonian frequently has been used as the starting point for adding additional interactions. Mele and Rice suggested [100] the commensurate charge density wave (CDW) to incommensurate CDW transition model. This model introduced a wide soliton band between the conduction and valence bands as the doping level is increased. In this model, disorder plays an important role to close the incommensurate Peierls gap and convert the system into a conductor. As the most highly conducting doped polymers are the most ordered, this mechanism is unlikely. Kivelson and Heeger later proposed that for polyacetylene there is a first order transition from the soliton lattice to the polaron lattice with increased doping [101]. Though a charged polaron band would be a half-filled band and thus metallic (in the absence of a further Peierls transition), later studies suggested that the infrared data was inconsistent with this model [102–104].

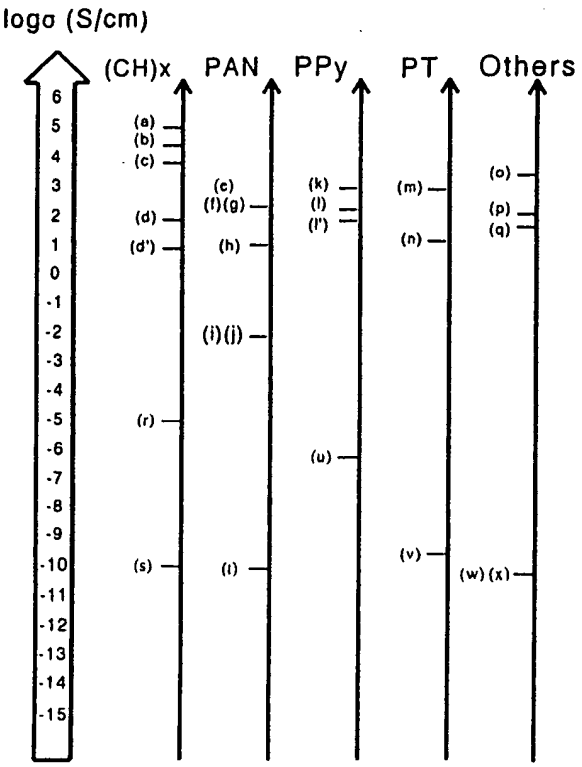

FIGURE 34.4. Overview of conductivity of conducting polymers at room temperature. (a) stretched $[CH(I_3)]_x$ (from Ref. 63), (b) stretched $[CH(I_3)]_x$ (from Ref. 64), (c) $[CH(I_3)]_x$ (from Ref. 65), (d) $[CH(I_3)]_x$ (from Ref. 17), (d') $[CH(I_3)]_x$ (from Ref. 83), (e) stretched PAN-HCl (from Ref. 71), (f) PAN-CSA from *m*-cresol (from Ref. 84), (g) PAN-CSA from *m*-cresol (from Ref. 73), (h) PAN derivative: poly(o-toluidine) POT-CSA fiber from *m*-cresol (from Ref. 85), (i) POT-HCl (from Ref. 86), (j) sulfonated PAN (from Ref. 87), (k) stretched $PPy(PF_6)$ (from Ref. 88), (l) $PPy(PF_6)$ and (l') PPy(TsO) (from Ref. 74, 89), (m) iodine doped poly(dodecylthiophene) (from Ref. 72), (n) $FeCl_4$ doped PT (from Ref. 90), (o) $PPV(H_2SO_4)$ (from Ref. 91), (p) $PPP(AsF_5)$ (from Ref. 92), (q) $^{84}Kr^+$ implanted (polyphenylenebenzobisoxazole) (from Ref. 93), (r) undoped *trans*-$(CH_x$ (from Ref. 94), (s) undoped *cis*-$(CH)_x$ (from Ref. 95), (t) undoped PAN (EB) (from Ref. 96), (u) undoped PPy (from Ref. 97), (v) undoped PT (from Ref. 90), (w) undoped PPV (from Ref. 98), (x) undoped PPP (from Ref. 92). The conductivity reported for the undoped polymers should be considered an upper limit due to the possibility of impurities.

Conwell and others have proposed that when long-range Coulomb interactions and screening are taken into account, the soliton band in *trans*-$(CH)_x$ overlaps the valence and conduction bands, giving a metallic state [52,53]. In contrast, Kivelson and Salkola have focused on the interchain interaction, which they show can lead to a simple metallic system with no residual Peierls interaction [105]. Baeriswyl, and others, have shown that in some limits the Coulomb interaction is sufficient to close the Peierls gap, giving a metallic state as well [8]. Epstein, *et al.* proposed that a disordered conducting state (not the metallic state) is stabilized in the presence of three-dimensional disorder [83]. Other more exotic schemes for the transition to the metallic state also have been proposed [106–109]. For the nondegenerate ground state conducting polymers, more emphasis has been placed on an empty (p-doped) or filled (n-doped) bipolaron energy band overlapping the valence or conduction band, respectively, giving rise to the metallic behavior [56]. Alternatively, a partially filled polaron (band) lattice metallic state [26,31,54,55,56,61,110,111] has been proposed for some materials.

34.2.3 Models for Localization and Metallic Conductivity

Much work has also focused on the nature of the carriers in the highly doped metallic state. Even though there are a high density of conduction electrons at the Fermi level for the highly doped state, the carriers may be spatially localized so they cannot participate in transport except through hopping. The prime source of localization which has been studied is structural disorder in the polymers [18]. X ray studies of these systems show that they are generally of modest crystallinity, with regions of the material which are more ordered while other regions are more disordered. Also, the fibrillar nature of many of the conducting poly-

mers may lead to localization by reducing the effective dimensionality of the electrons delocalized in a bundle of polymer chains [112].

In a perfect crystal with periodic potentials, electron wave functions form delocalized Bloch waves [113]. Impurities and lattice defects in disordered systems introduce backward scattering. Anderson studied this phenomenon in terms of a localization effect and the disorder induced metal-insulator transition [114]. It is well known that the electronic structure of the system strongly depends on the degree of disorder. The energy fluctuation in the random potentials broadens the bandwidth and creates smooth "band tails." Due to these band tails, the original band gap between the conduction and the valence bands of a semiconductor may be closed. The ramifications, a finite density of states $N(E_F)$ produced at the Fermi level E_F between mobility edges, were discussed by Mott [115]. When the Fermi level lies in the localized region, the conductivity at zero temperature is zero even for a system with a finite density of states. The Mott variable range hopping (VRH) model is applicable to systems with strong disorder such that ΔV (disorder energy)$\gg B$ (band width) [115]. The general form of the temperature dependent conductivity of Mott's model is described as

$$\sigma=\sigma_0 \exp\left[-\left(\frac{T_0}{T}\right)^{1/d+1}\right], \qquad (34.1)$$

where d is the dimensionality and, for three-dimensional systems, $T_0=c/k_B N(E_F)L^3$ (c is the proportionality constant, k_B the Boltzman constant, and L the localization length). If the Fermi level is at an energy such that the electronic states are extended, then finite conductivity at zero temperature is expected. This model assumes that substantial disorder is homogeneous throughout the isotropic three-dimensional sample. For three-dimensional materials near the insulator-metal transition, the Ioffe-Regel condition, $k_F l \sim 1$ where k_F is the Fermi wavevector and l is the mean free path, is satisfied, implying a very short localization length and a very short scattering time. Other external parameters such as magnetic field or pressure can affect the localization/delocalization transition and the localization lengths. This model has received much experimental attention for doped [83,116–118] and ion implanted polymers [93].

In Mott's model, electron correlations are neglected as for the classical Fermi liquid. Efros and Shklovskii pointed out that the interactions between localized electrons and holes play an important role in the hopping transport, especially at low temperature [119], changing the expected temperature dependence of the conductivity to

$$\sigma=\sigma_0 \exp\left[-\left(\frac{T_0'}{T}\right)^{1/2}\right], \qquad (34.2)$$

where $T_0'=e^2/\epsilon L$ (e is the electron charge, and ϵ is the dielectric constant).

It is well known for a one-dimensional metallic chain that the localization of charge carriers arises for even weak disorder because of quantum interference of static backscattering [115]. In contrast, strong disorder (the mean free path is comparable with the Fermi wavelength) is required for localization in three-dimensional systems. This consequently requires a short transport time, and hence low σ_{DC} at room temperature. Anderson localization therefore is unlikely for the partially crystalline chain structured doped conducting polymers. The localization effects in the inhomogeneously disordered (partially crystalline) conducting polymers may originate from the one-dimensional localization in the disordered regions [73,74,120].

Prigodin and Efetov studied the insulator-metal transition of conducting polymers using a random metallic network (RMN) model [112] to represent weakly connected, fibrous bundles of metallic chains. In this zero temperature model, the phase transition is a function of the cross-sectional capture between fibers (α), and the product ($\rho=pR_{loc}$) of the localization radius (R_{loc}) and the concentration of crosslinks between fibers (p). The metallic state can be induced by strengthening the interchain (or interfibril) interaction (increasing α), increasing the density of crosslinks between fibers (increasing p), or increasing the localization length (increasing R_{loc}). This model developed for contacts between fibers comprised of parallel polymer chains can be generalized to the three-dimensional delocalization transition that occurs in inhomogeneously disordered (partially crystalline) nonfibrillar polymers: as the strength of connection between ordered or crystalline regions (α) is increased, the density of interconnections between ordered or crystalline regions (p) increases, and the localization length within the disordered regions (R_{loc}) increases.

The inhomogeneous disorder model was expanded [120] to account for the temperature dependence of the conductivity. Within this model, conduction electrons are three-dimensionally delocalized in the "crystalline" ordered regions (though the effects of paracrystalline disorder may limit delocalization within these regions [121]). In order to transit between ordered regions, the conduction electrons must diffuse along electronically isolated chains through the disordered regions where the electrons readily become localized. Phonon-induced delocalization increases the conductivity with increasing temperature. This model accounts for localized behavior at low temperature despite conductivities at room temperature in excess of the Mott minimum conductivity. Three-dimensional crystalline order facilitates delocalization. It has been shown [122] that nematic-like order can also increase delocalization, though less effectively.

For conventional metals, the electrical transport properties can be described by the Drude model [123,124] within which electrons are treated as free particles in a gas with a single scattering time τ. Despite its simplified assumptions, the Drude model explains high and frequency independent conductivity from dc to the microwave ($\sim 10^{10}$ Hz)

frequency range, and a real part of the dielectric constant (ϵ_r) which is negative below the screened plasma frequency ($\omega_p^2 = 4\pi n e^2/m^* \epsilon_b$; n is the density of carriers, m^* is the carrier effective mass, and ϵ_b is the background dielectric constant) [124]. Within the Drude model the real (ϵ_r) and imaginary part (ϵ_i) of the dielectric function are

$$\epsilon_r = \epsilon_b - \frac{\omega_p^2 \tau^2}{1+\omega^2\tau^2}, \tag{34.3}$$

$$\epsilon_i = \frac{\omega_p^2 \tau}{\omega(1+\omega^2\tau^2)}, \tag{34.4}$$

where ω is the external frequency.

In low frequency limit ($\omega\tau \ll 1$), the Drude response can be deduced as

$$\epsilon_r \simeq -\omega_p^2\tau^2, \tag{34.5}$$

$$\epsilon_i \simeq \omega_p^2\tau/\omega. \tag{34.6}$$

34.3 STRUCTURAL ORDER

Each of the conducting polymer systems exhibits different local structures and a wide range of local orders depending upon the synthesis and processing routes used [18]. The typical fraction of crystallinity and the crystalline coherence lengths for typical samples of three of the most intensively studied highly conducting polymer systems are given in Tables 34.1 and 34.2. The synthetic route, processing procedure, and dopant counterion also will affect the crystal structure as well as the percent crystallinity. For both p and n doping of polyacetylene, the polymer forms a number of different structures (stages) as a function of doping level [19,20,125]. Similar results are found for doped PPV [126]. There is less evidence for intermediate stages at various dopant/polymer stoichiometries for the other conducting polymers. Instead, data support formation of inhomogeneous regions of fully doped polymer which increase in number with increasing doping. Doped polyacetylene can be as much as 80–90% crystalline.

Polyaniline forms a rich set of structures dependent upon the processing sequence and dopant [18,62,127–132]. Generally, doped polyaniline obtained from solution in the doped (conducting salt) form exhibits a local crystalline order of type emeraldine salt-I, ES-I. In contrast, polyaniline obtained by doping powder or films cast as the base form from solution are of the ES-II type [62,122,131–133]. Both preparation methods lead to between a few percent and about 50% crystallinity dependent upon details of the processing route. In addition, there are significant differences in the type of local order that exist in the disordered regions between the crystalline ordered regions, varying from coil-like, to expanded coil-like, to more rod-like [133–135]. For undoped and doped polyaniline, short range local order in the disordered regions resembles that in the ordered regions [18,133]. Table 34.1 summarizes the fraction of crystallinity and the x ray coherence lengths of the various doped polyaniline systems, while Table 34.2 compares the fraction of crystallinity and x ray coherence lengths for selected doped polyacetylene, polypyrrole, and polyaniline samples.

Similarly, the degree of local order varies for polypyrrole dependent upon the preparation method, with the degree of crystallinity varying from nearly completely disordered up to ~50% crystalline [18,136]. In contrast to polyaniline, the local order in the disordered regions of polypyrrole does not resemble that in the ordered regions [18].

The percent crystallinity for doped polyacetylene is usually larger than that of doped polyaniline or doped polypyrrole [18,137]. For each of these systems, the coherence length within the doped crystallographic regions generally is no more than 50–75 Å along the chain direction with smaller values in the perpendicular direction. It has been proposed that these coherent crystalline regions form metallic islands and the disordered weak links between

TABLE 34.1. *Typical percent crystallinity and crystalline coherence lengths (ξ (Å)) of various polyaniline materials obtained from x ray diffraction experiments.*

Materials	Crystallinity (%)	$\xi_{\parallel}$ (Å)	$\xi_{\perp}^{b}$ (Å)	$\xi_{\perp}^{a}$ (Å)
^{i} XPAN-ES^{a} (3.5×) [73,132]	~45	73	57	29
^{h} XPAN-ES^{a} (3.5×) [73,132]	~40	64	47	23
^{h} XPAN-ES^{b} (5.5×) [73,132]	~35	57	45	21
PAN-ES^{b} (4×) [73,132]	~30	52	42	23
^{n} XPAN-ES^{b} (1×) [73,132]	<15		15	

[a]High molecular weight samples. XPAN-ES represents the "physically crosslinked" polyaniline emeraline salt. Note that *i*, *h*, and *n* refer to intermediate, high, and non-crosslinked samples, respectively. The stretch ratio (l/l_0) is given in parentheses (e.g., 3.5×). Note that $\xi_{\perp}^{a}$, $\xi_{\perp}^{b}$, and $\xi_{\parallel}$ are obtained from full width at half maximums of (200), (010), and (002) ES-II reflections, respectively.
[b]Low molecular weight samples.

TABLE 34.2. *Typical percent crystallinity and crystallographic coherence lengths (ξ (Å)) for highly conducting polymer systems.*[a]

Highly conducting polymer	Crystallinity (%)	$\xi_{\parallel}$[a] (Å)	$\xi_{\perp}$[a] (Å)
T-$(CH(I_3)_y)_x$ [18,137][a]	~80	50	35
PPy-PF6 [18,136][b]	~50	20	20
PAN-CSA (*m*-cresol) [18][c]	~50	50	30

[a]The terms ∥ and ⊥ refer to parallel and perpendicular to the chain direction, respectively.
[b]T-$(CH(I_3)_y)_x$ is the heavily iodine doped Tsukamoto polyacetylene.
[c]PPy-PF6 is the hexafluorophosphate doped polypyrrole.
[d]PAN-CSA (*m*-cresol) is the camphor sulfonic acid doped polyaniline cast from *m*-cresol solvent.

more ordered regions are areas where conduction electrons are subject to localization, as expected for charges moving through isolated one-dimensional chains. That is, for each very highly conducting polymer system studied, there are regions of one-dimensional electronic character through which conduction electrons must pass [75].

34.4 DENSITY OF STATES

Magnetic susceptibility studies identify the charge storage mechanism at low doping levels, as well as the density of states at the Fermi level and the density of localized "Curie" spins at higher dopant levels. For $(CH)_x$, spinless solitons dominate at low doping levels [76,78]. In contrast, spin 1/2 polarons and spinless bipolarons are present in nondegenerate systems at low doping levels [7,33,138]. At high doping levels, the highest conducting doped polyacetylene, polypyrrole, polyaniline, polythiophene, and polyparaphenylenes are reported to have finite densities of states at the Fermi level [$N(E_F)$]. Typical literature values of $N(E_F)$ [27,61,62,71,74–76,78,79,138–148] for each of these systems are presented in Table 34.3. Having the Fermi level in a partially filled conduction band results in Pauli susceptibility ($\chi_{Pauli}=2\mu_B^2N(E_F)$) and enables metallic conduction. The magnitude of χ_{Pauli} depends on the structural order and morphology of the polymers as this affects the uniformity of the doping. It is noted that the values of $N(E_F)$ in Table 34.3 have not been scaled to the percent crystallinity. Hence the intrinsic density of states in each of the ordered polymers may be larger than indicated.

For the earliest studied iodine doped Shirakawa [76,78,139] and Naarmann [140] $(CH)_x$, Fig. 34.5, $N(E_F)\sim0.1$ states/eV-C for doping levels above ~4–6% doping level. With the recently studied Tsukamoto [75,142] $(CH)_x$, which has a more compact morphology, a higher doping level was attained resulting in $N(E_F)\sim0.2-0.3$ states/eV-C, Fig. 34.5, indicating that the doping was more homogeneous.

For PAN, $N(E_F)$ is finite and has been shown to increase with the level of protonic acid doping and the volume fraction of crystalline material for both the ES-I, Fig. 34.6, and ES-II, Fig. 34.7, structure [61,62]. The $N(E_F)$ differ for ES-I HCl and ES-II HCl, being 0.26 states/eV-(C+N), and 0.083 states/eV-(C+N), respectively [143]. For highly conducting PAN-CSA (*m*-cresol) [79], $N(E_F)\sim0.07$ states/eV-(C+N). Recently, a differently prepared stretched PAN doped with HCl was reported to have a much higher $N(E_F)$,~1.4 states/eV-(C+N) [71]. Some solutions of PAN-CSA have been reported to have a Pauli-like susceptibility [144].

Highly conducting doped polypyrrole has a large χ_{Pauli} [74]. The samples initially studied typically had conductivities in the range of ~1–10 S/cm with little crystallinity; for these materials, $N(E_F)\leq0.01$ states/eV-C [145]. Later studies on BF_4 doped PPy [138,146] indicated $N(E_F)\sim0.045$ states/eV-C. However, these films were not structurally characterized. A coordinated study of PPy doped with hexafluorophosphate [PPy(PF_6)] and toluene sulfonate [PPy(TsO)] [74] shows that for the more highly crystalline (50%), higher conductivity ($\sigma_{DC}\sim300$ S/cm) PPy(PF_6), $N(E_F)\sim0.2$ states/eV-C, similar to what was found for highly conducting iodine doped Tsukamoto $(CH)_x$. For less crystalline (25%), lower conductivity ($\sigma_{DC}\sim120$ S/cm) PPy(TsO), $N(E_F)\sim0.05$ states/eV-C. Fig. 34.8 contrasts the density of states [$N(E_F)=\chi_{Pauli}/2\mu_B^2$]

TABLE 34.3. *Typical χ_{Pauli} and $N(E_F)$ for highly conducting polymer systems.*

Material	χ^{Pauli}	$N(E_F)$
$[CH(I_3)_y]_x$ [75,142,160]	1.1×10^{-5} emu/mol-C	0.33 states/eV-C
$[CH(I_3)_y]_x$ [76,139,140]	2.9×10^{-6} emu/mol-C	0.09 states/eV-C
$[CH(ClO_4)_y]_x$ [141]	3.3×10^{-6} emu/mol-C	0.11 states/eV-C
$[CH(ClO_4)_y]_x$ [139]	2.3×10^{-6} emu/mol-C	0.08 states/eV-C
$[CH(Na)_y]_x$ [139]	2.0×10^{-6} emu/mol-C	0.07 states/eV-C
PAN(HCl) ES-I [61,143]	7.9×10^{-6} emu/mol-(C+N)	0.26 states/eV-(C+N)
PAN(HCl) ES-II [62,143]	2.5×10^{-6} emu/mol-(C+N)	0.083 states/eV-(C+N)
PAN(HCl) [71]	4.0×10^{-5} emu/mol-(C+N)	1.4 states/eV-(C+N)
PAN(CSA) [79]	2.1×10^{-6} emu/mol-(C+N)	0.07 states/eV-(C+N)
PAN(SO_3) ("SPAN") [87]	1.7×10^{-6} emu/mol-(C+N)	0.06 states/eV-(C+N)
POT(HCl) [121]	3.9×10^{-6} emu/mol-(C+N)	0.13 states/eV-(C+N)
PPy(PF_6) [74]	7×10^{-6} emu/mol-C	0.20 states/eV-C
PPy(TsO) [74]	1.8×10^{-6} emu/mol-C	0.05 states/eV-C
PPy(BF_4) [146]	1.7×10^{-6} emu/mol-C	0.05 states/eV-C
PT(AsF_6) [27]	7.5×10^{-6} emu/mol-C	0.23 states/eV-C
PT(BF_4) [146]	1.5×10^{-6} emu/mol-C	0.05 states/eV-C
PPP(AsF_6) [147]	1.5×10^{-6} emu/mol-C	0.05 states/eV-C
C_2H_5O-PPV(BF_4) [148]	$\leq1\times10^{-6}$ emu/mol-C	0.03 states/eV-C

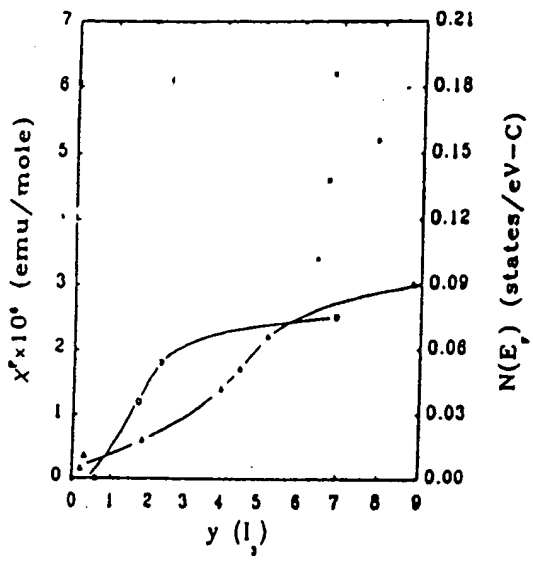

FIGURE 34.5. Pauli susceptibility and density of states as a function of I_3 doping level for an oriented ($l/l_0 \sim 6$) Naarmann polyacetylene (triangles) (N-$(CH)_x$) (from Ref. 135), unoriented Shirakawa polyacetylene (circles) (S-$(CH)_x$) (from Ref. 140), and Tsukamoto polyacetylene (x) (T-$(CH)_x$) (from Ref. 75, 160).

and number of localized Curie-like spins measured for the PPy-PF_6 and PPy-TsO compounds [74]. The more metallic PPy-PF_6 clearly has the larger χ_{Pauli} and the smaller number of localized Curie spins (independent polarons).

For doped polythiophene, there is variation of the doping

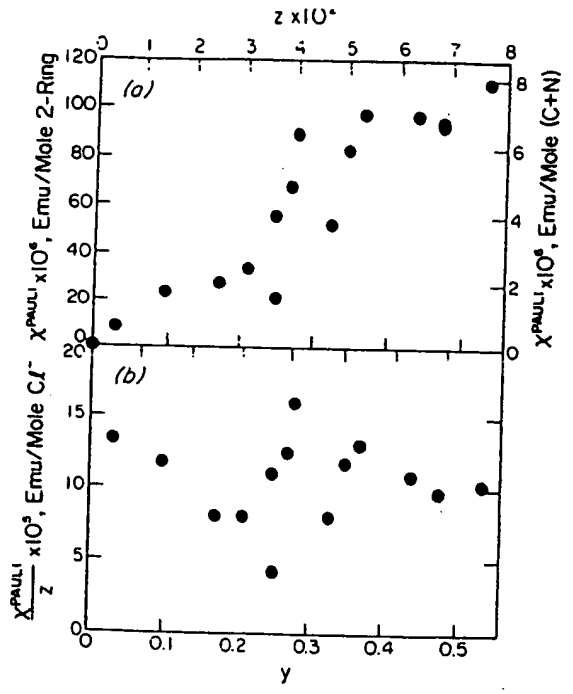

FIGURE 34.6. $N(E_F)$ versus doping level for PAN-HCl, ES-I structure. The lower curve presents χ_{Pauli} normalized to the doping level (from Ref. 61).

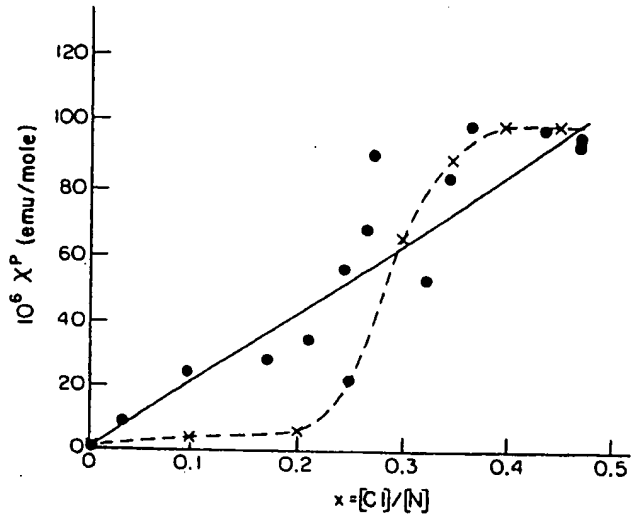

FIGURE 34.7. $N(E_F)$ versus doping level for PAN-HCl, ES-II structure (dashed line). The closed circles are for HCl doping of the ES-I structure (from Ref. 62).

level attained with different dopants. For BF_4 doped PT [146], $N(E_F) \sim 0.05$ states/eV-C at the 4–8% dopant level. For PT(AsF_6) [27], the doping is inhomogeneous until 26 mol% where $N(E_F) \sim 0.23$ states/eV-C.

For PPP, a metallic density of states of $N(E_F) \sim 0.05$ states/eV-C has been reported for doping with AsF_6 [147]. There are no reports in the literature concerning the temperature dependence of the susceptibility of doped PPV. However, if the reported room temperature magnetic susceptibility measured of BF_4 doped poly(2,5-diethoxy-p-phenylene-vinylene) [C_2H_5O-PPV(BF_4)] [143] is entirely due to a Pauli contribution, an upper estimate of $N(E_F)$ is 0.03 states/eV-C.

In sum, for each of these systems the metallic density of

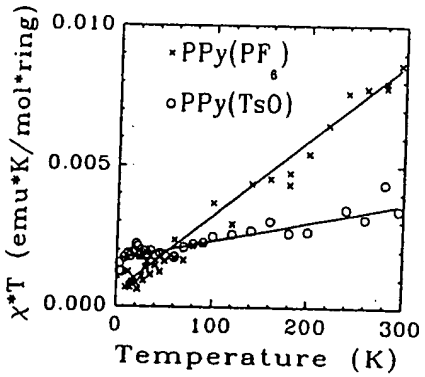

FIGURE 34.8. χT versus T for PPy-PF_6 and Ppy-TsO (from Ref. 74). Note that assuming $\chi = (\chi_{Pauli} + \chi_{Curie})$ and that χ_{Pauli} is T independent while $\chi_{Curie} \propto T^{-1}$, PPy-$PF_6$ has the larger regions of metallic density of states while the PPy-TsO system has a greater density of localized (independent polaron) spins.

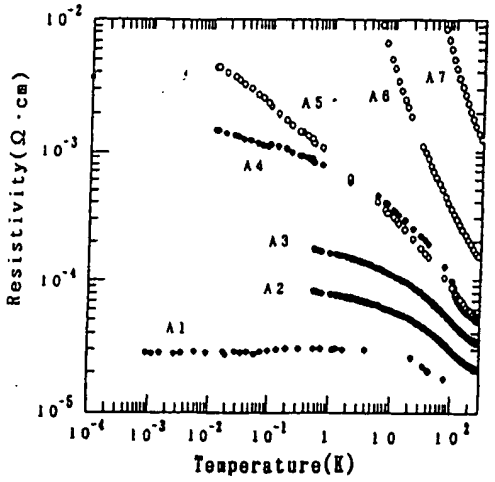

FIGURE 34.9. Temperature dependence of the resistivity for various heavily iodine doped poly-acetylenes represented in a log ρ versus log T scheme (from Ref. 70).

states at the Fermi level varies substantially. Where data are present, the Pauli susceptibility increases with increasing three-dimensional or nematic order.

34.5 TEMPERATURE DEPENDENT CONDUCTIVITY AND MAGNETORESISTANCE

34.5.1 Conductivity

The temperature dependent dc conductivity, $\sigma_{dc}(T)$, provides a direct probe of the macroscopic charge conduction through the less conducting regions. Recent advances

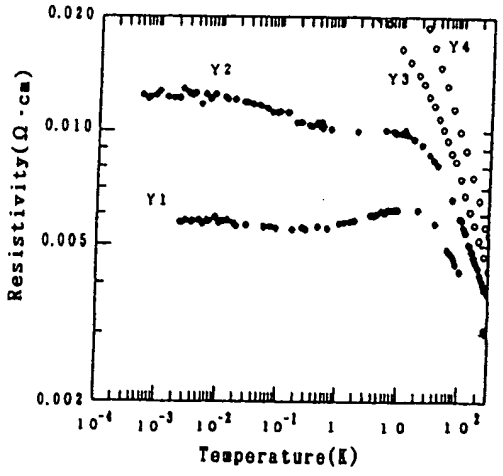

FIGURE 34.10. Temperature dependence of the resistivity for PF_6 and BF_6 doped polypyrroles represented in a log ρ versus log T scheme (from Ref. 70).

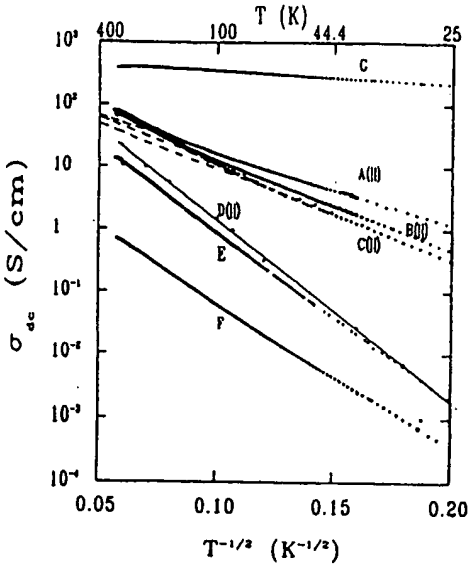

FIGURE 34.11. $\sigma_{dc}(T)$ for "crosslinked" PAN-ES, PAN-CSA ($CHCl_3$, and PAN-CSA (*m*-cresol) samples (from Ref. 73). The dashed straight lines are based upon the quasi 1D VRH model. Note here "crosslinks" refers to physical crosslinks (microcrystalline regions) not chemical crosslinks (covalent bonds).

in chemical processing have resulted in higher conductivity and crystallinity for conducting polymers.

Ishiguro, *et al.* reported the temperature dependent resistivity $[\rho(T)]$ of heavily iodine doped $(CH)_x$ and hexafluorophosphate (PF_6) doped PPy down to mK range as a function of aging (disorder), Figs. 34.9 and 34.10, respectively [70]. The highest σ_{dc} at room temperature reported in this study is $\sim 5\times 10^4$ S/cm for I_3 doped T-$(CH)_x$ and $\sim 10^3$ S/cm for the highest conducting PPy(PF_6). For both of these materials, the conductivity decreases with decreasing temperature to a minimum at $T_m \sim 10$ K. Below T_m, σ increases by ~20% and then is constant to 1 mK. Some highly conducting preparations of PAN-CSA show similar behavior [82].

Hydrochloric acid as well as camphor sulfonic acid doped polyaniline prepared in chloroform often have log σ proportional to $T^{-1/2}$ as expected for quasi-one-dimensional variable range hopping (VRH), Fig. 34.11, [73,121,143]:

$$\sigma = \sigma_0 \exp[-(T_0/T)^{1/2}], \qquad (34.7)$$

where $T_0 = 16/[k_B N(E_F) L z]$. Here L is the one-dimensional localization length and z the number of nearest neighbor chains. Generally, the higher conductivity samples have a weaker temperature dependence at low temperatures ($T_0 \sim 700$–1000 K for $T < 80$ K), and lower conductivity samples a stronger temperature dependence ($T_0 \sim 4000$ K) [73]. The smaller T_0 for the more highly conducting samples has been associated with weaker localization due to improved intrachain and interchain order.

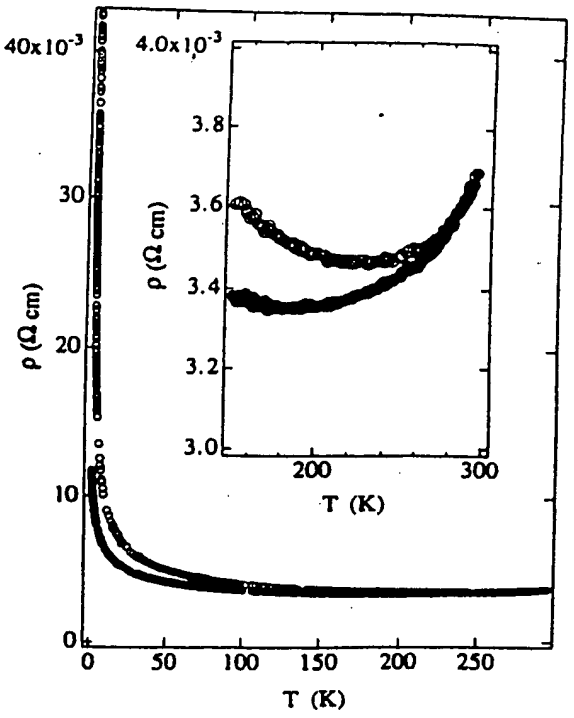

FIGURE 34.12. Resistivity versus temperature for PAN-CSA (*m*-cresol). The inset shows the resistivity minima on an expanded scale (from Ref. 116).

Higher conducting polyaniline films that were prepared from solutions of PAN and HCSA in *m*-cresol have an intrinsic metal-like temperature dependence at room temperature to ~200 K below which the conductivity decreases slowly, Fig. 34.12. It was shown that this metal-like behavior for T>200 K can occur in the presence of one-dimensional localization when the phonon backscattering rate becomes larger than the impurity scattering rate [120]. A similar temperature dependence for conductivity has been reported for $FeCl_3$ doped polyacetylene [149].

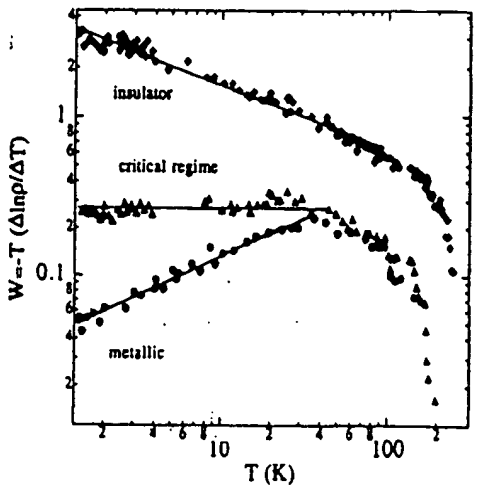

FIGURE 34.13. *W* plot for PAN-CSA (*m*-cresol) for samples in the insulating, critical, and metallic regime (from Ref. 111).

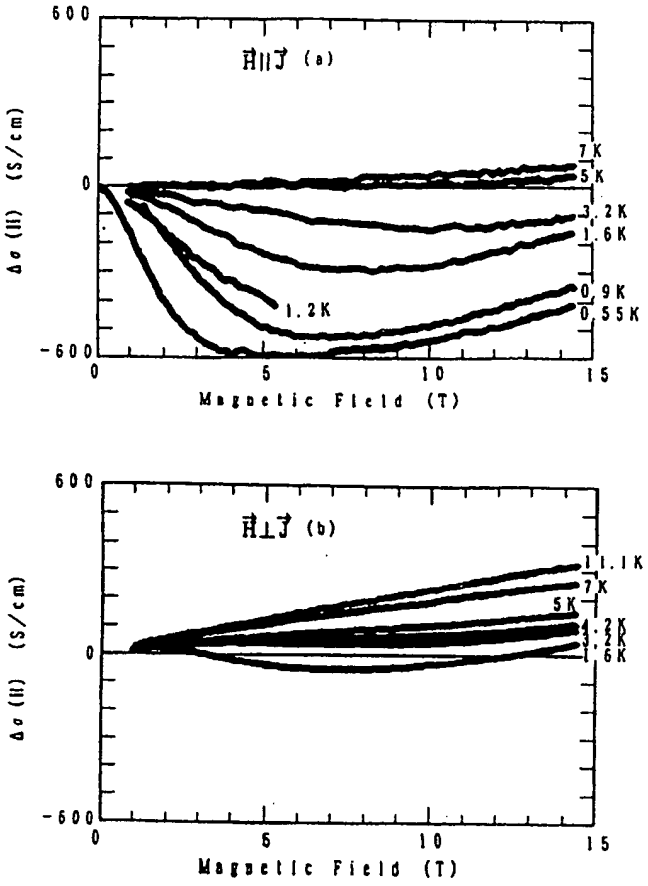

FIGURE 34.14. Magnetic field dependence of the conductivity increment $\Delta\sigma(H)$ at various temperatures for heavily iodine doped T-$(CH)_x$ (from Ref. 155).

For PAN-CSA [116,120], $PPy(PF_6)$ [74,118], and iodine doped $(CH)_x$ [150], the proximity of the material to the insulator-metal transition can be gauged by the resistivity ratio $\rho(1.4K)/\rho(300K)$ and a plot of the reduced activation energy: $W=-Tdln(\rho(T))/dT$ [151]. For a conductor close to the insulator-metal transition, the resistivity follows a power law behavior with T [152]; for a critical regime sample, the plot of log W versus log T approaches $T=0K$ at a constant value. The plot of log W vs log T for a critical sample provides a dividing line between the plot of log W versus log T for insulating hopping behavior which increases with decreasing T (i.e., the slope of log W versus log T is equal to γ if $\sigma \propto exp(T_0/T)^{\gamma}$) and the plot of log W versus log T for metallic samples which decreases with decreasing T. The W plots for selected PAN-CSA materials are shown in Fig. 34.13.

34.5.2 Magnetoresistance

The charge transport can be changed in the presence of an external magnetic field because of the destruction of

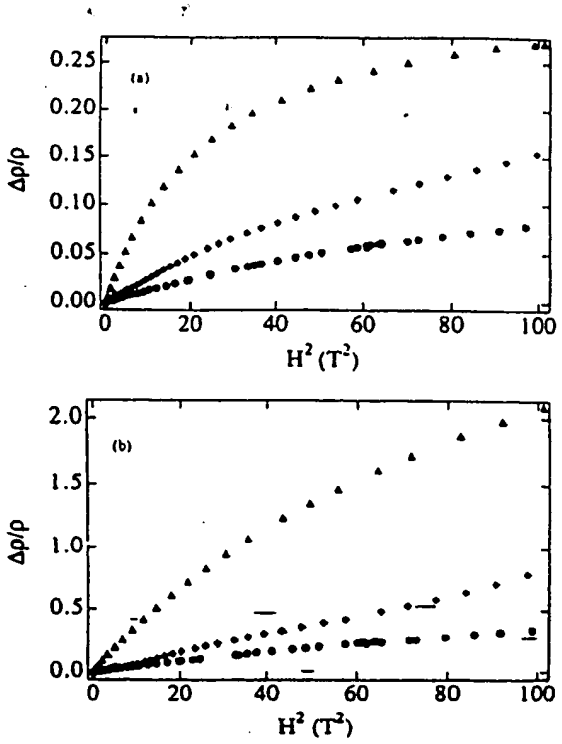

FIGURE 34.15. $\Delta\rho/\rho$ versus H^2 for PAN-CSA (*m*-cresol): (a) In the critical regimes; [$\rho(T) \propto T^{-0.26}$, 4.2 K (solid circles), 2.5 K (solid diamonds), and 1.4 K (solid triangles); (b) in the insulating regime (follows three-dimensional VRH model), 4.2 K (solid circles), 2.5 K (solid diamonds), and 1.4 K (solid triangles)] (from Ref. 116).

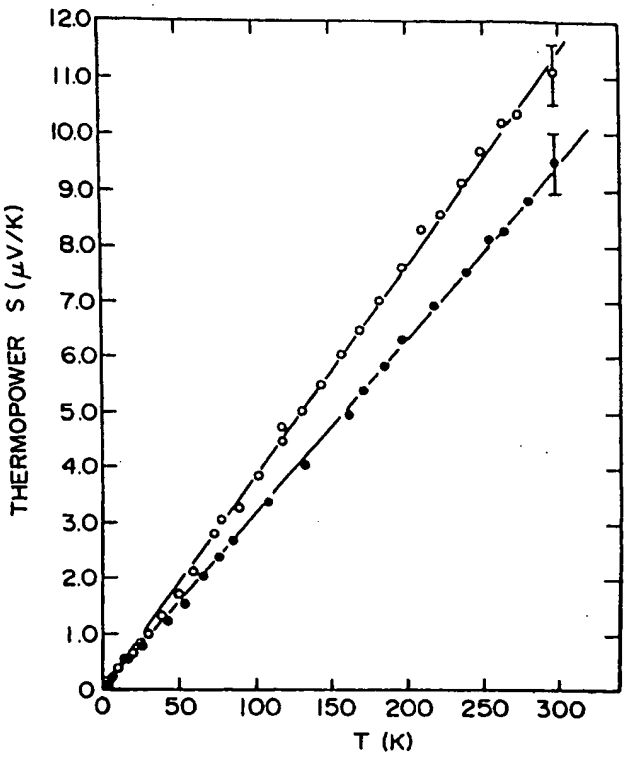

FIGURE 34.17. Temperature dependence of the thermoelectric power in unstretched (solid circles) heavily AsF_5 doped polyacetylene and stretched ($l/l_0 \sim 3.2$, open circles) ones (from Ref. 80(b)).

time-reversal symmetry, i.e., a total phase difference between two paths is created by the magnetic field [153]. The magnetoresistance is more easily detected at low temperature because of large localization effects. The fractional change of resistivity in the presence of a magnetic field, $\Delta\rho/\rho$, can be either positive or negative. A negative magnetoresistance can originate from localization effects

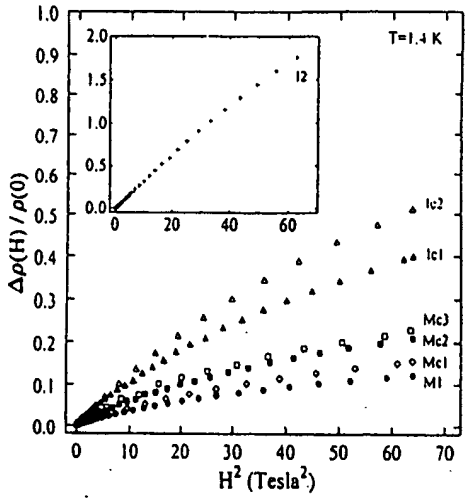

FIGURE 34.16. Magnetoresistance of doped polypyrroles (from Ref. 113). The inset shows the magnetoresistance for a less highly conducting doped PPy than in the main figure.

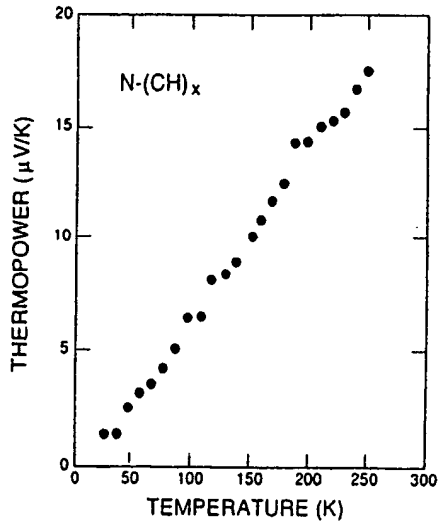

FIGURE 34.18. Thermoelectric power of stretched heavily iodine doped $N\text{-}(CH)_x$ film versus temperature measured parallel to the stretched axis (from Ref. 81).

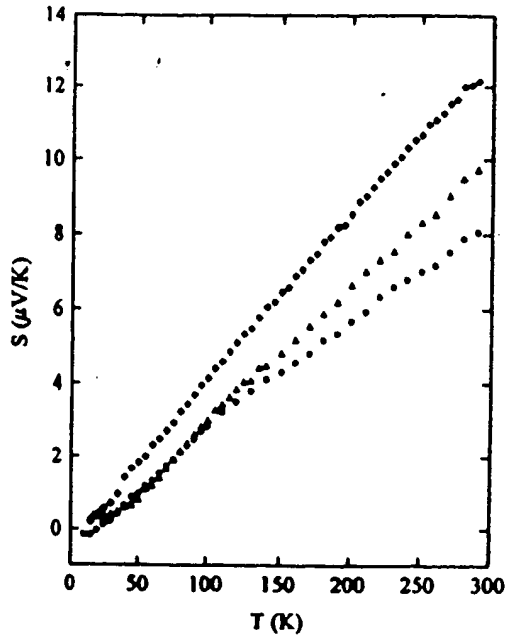

FIGURE 34.19. Temperature dependence of thermoelectric power of PAN-CSA (*m*-cresol) samples: different symbols refer to materials prepared in different casting conditions (from Ref. 117).

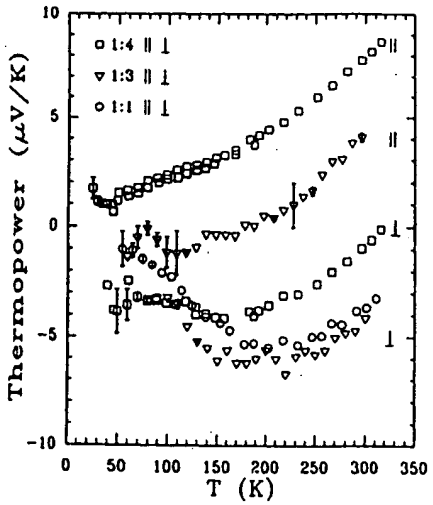

FIGURE 34.21. Comparison of temperature dependence of thermoelectric power of HCl doped PAN-ES samples (from Ref. 143).

caused by magnetic field-related dephasing. A field-dependent cutoff length $L_H = \sqrt{\hbar c/eH}$ where c is the speed of light is important at high magnetic fields [153]. A positive magnetoresistance is detected when the mobility edge E_c is shifted by the external magnetic field [154]. For an impurity conduction mechanism, the wave functions of the impurity electrons are compressed in the transverse direction by the magnetic field, leading to an enhancement of localization effects, which also induces a positive magnetoresistance [153].

Figures 34.14, 34.15, and 34.16 show examples [116,118,155] of the magnetoresistance of doped polyacetylene, polypyrrole, and polyaniline samples at low temperatures. A wide range of behaviors is observed. The variation in magnetoresistance for conducting polymers is closely related to the magnitude and temperature dependence of the conductivity in the absence of a magnetic field. For highly conducting doped $(CH)_x$, a negative magnetoresistance is

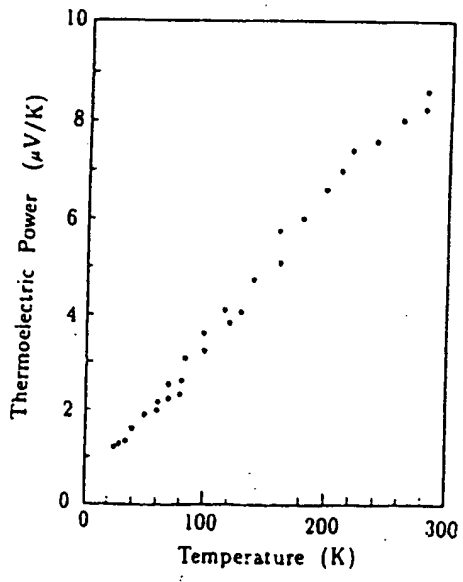

FIGURE 34.20. Temperature dependence of thermoelectric power of PF_6 doped polypyrrole (from Ref. 159).

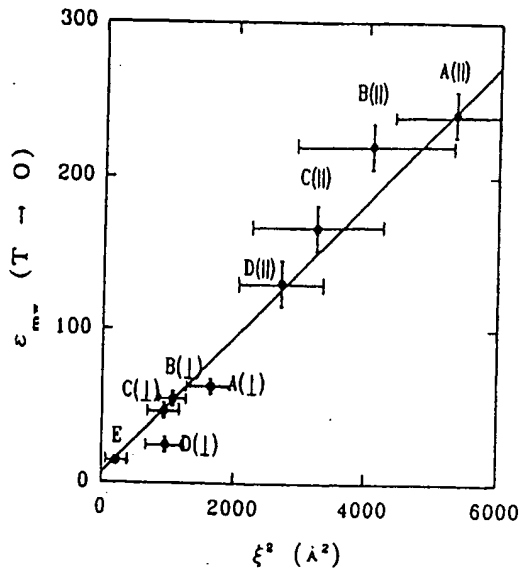

FIGURE 34.22. ϵ_{mw} (6.5×10^9 Hz, $T\to0$) vs ξ^2 for HCl doped PAN-ES ($\xi_\perp^2 = \xi_{\perp,a}\times\xi_{\perp,b}$) (from Ref. 73).

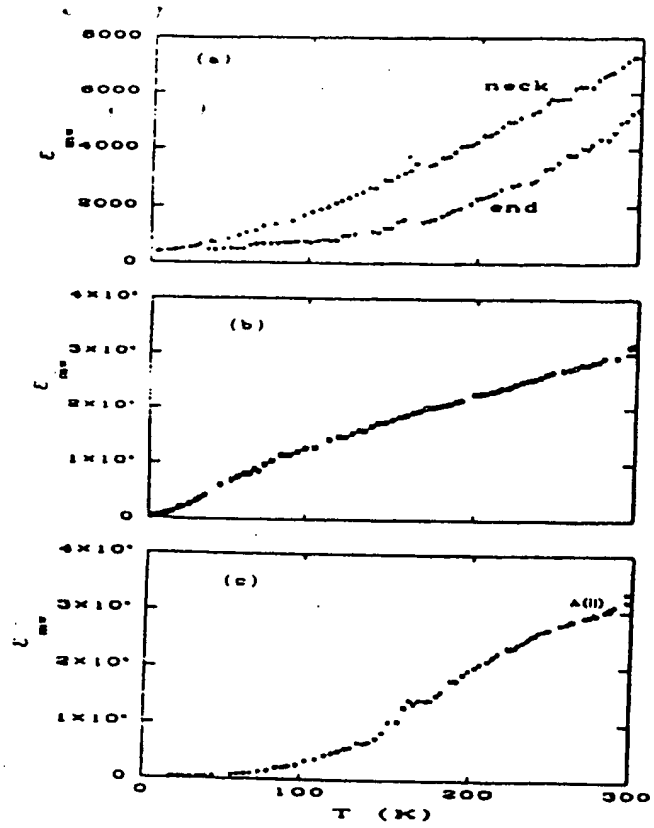

FIGURE 34.23. ϵ_{mw} (6.5×10^9 Hz) versus temperature for modestly conducting doped polymers. (a) I_3 doped Tsukamoto polyacetylene (unstretched end and modestly stretched neck portions of sample) (from Ref. 75, 160), (b) unstretched PPy-TsO (from Ref. 74), and (c) intermediate "crosslinked" 3.5 times stretched HCl doped PAN-ES (from Ref. 73).

observed [81,155] in both the parallel and perpendicular directions (Fig. 34.14) which is attributed to quantum interference though the magnitude of the magnetoresistance in the parallel direction is relatively insensitive to the magnetic field. For highly conducting PPy(PF_6) and PAN-CSA materials, the magnetoresistance is usually positive, (Figs. 34.15 and 34.16), which was interpreted as a shift of the mobility edge in the presence of a magnetic field.

34.6 THERMOELECTRIC POWER

The results of thermoelectric power experiments determine the sign of the conducting charge, either electron-like (for a negative thermoelectric power) or hole-like (for a positive thermoelectric power). In terms of band theory, the positive or negative thermoelectric power implies p-type or n-type doping of a system, respectively. For inhomogeneous conducting polymers, there are several different contributions to the total thermoelectric power [156,157].

When the conductivity is determined by the motion of charge carriers near the Fermi level, where states are metallic (delocalized), the thermoelectric power is [115]

$$S(T)=\frac{2\pi^2}{3}\frac{k_B^2T}{e}\left.\frac{d\ln N(E)}{dE}\right|_{E=E_F} \tag{34.8}$$

Assuming a weak energy dependence of the density of states $N(E_F)$, the thermoelectric power increases linearly as the temperature increases.

When the conduction is determined by three-dimensional VRH, $S(T)\propto\sqrt{T}$ [115]. For a quasi one-dimensional VRH case, the thermoelectric power due to the interchain motion is constant [143] while that due to intrachain hopping is $\propto 1/T$, similar to that of doped semiconductors [115].

Park, *et al.* [80] and Javadi *et al.* [81] reported metallic thermoelectric power [$S(T)\propto T$] for heavily doped highly conducting polyacetylene (Figs. 34.17 and 34.18) though VRH-type $S(T)\propto\sqrt{T}$ had been reported earlier for poorly conducting polyacetylene [83]. Similarly, highly conducting forms of polyaniline and polypyrrole have $S(T)\propto T$, Fig. 34.19 [117,158] and Fig. 34.20 [154], while more disordered materials show nonlinear temperature dependent behavior, which might include the three-dimensional or quasi-one-dimensional VRH contributions. Figure 34.21 [143] shows the nonlinear $S(T)$ of some hydrochloride doped polyaniline materials.

34.7 MICROWAVE DIELECTRIC CONSTANT

The microwave frequency dielectric constant provides a measure of the charge delocalization in individual samples. Fig. 34.22 presents [73] the low temperature dielectric constant, ϵ_{mw}, for a series of emeraldine hydrochloride samples plotted against the square of the crystalline coherence length, ξ (as measured by x ray diffraction). For low temperatures, ϵ_{mw} is proportional to ξ^2 independent of the direction of orientation of the sample with regard to the microwave frequency electric field. This demonstrates that the charge is delocalized three-dimensionally within the crystalline regions of these samples. Using a simple metallic box model [73,143],

$$\epsilon=\epsilon_\infty+(2^{9/2}/\pi^3)e^2N(E_F)L^2, \tag{34.9}$$

and taking for the low temperature localization length the x ray crystalline correlation length determined by x ray diffraction, $N(E_F)\simeq 1.23$ state/(eV 2-rings) (0.088 state/eV-(C+N)) for PAN-HCl. This compares very favorably with the value obtained from magnetic susceptibility experiments [61].

A positive microwave frequency dielectric constant is also found for modestly conducting iodine doped unstretched and modestly stretched Tsukamoto polyacetylene [75] and for unstretched PPy-TsO [74], Fig. 34.23(a) and (b). Using Eq. 34.9, the size of the low temperature metallic box, L, can be determined. Table 34.4 summarizes the low temperature microwave dielectric constant for

TABLE 34.4. *Low temperature dielectric constant, $\epsilon_{mw}(T\to 0)$ and derived metallic box size, $L(T\to 0)$, compared to the x ray diffraction determined coherence length, ξ, for typical modestly conducting polymers.*

Modestly conducting polymer systems	$\epsilon_{mw}(T\to 0)$	$L(T\to 0)$ (Å)	ξ (Å)
T-$(CH(I_3)_y)_x$ [75]	~400	~170	not measured
PPy-TsO [74]	~20	~25	~15
PAN-CSA ($CHCl_3$) [73,75]	~30	~24	$\xi_\parallel$~35, $\xi_\perp$~25

typical modestly conducting doped polymers and the corresponding metallic box size calculated using Eq. 34.9. In each case L is approximately the size expected from x ray diffraction studies of the structural coherence length, ξ.

An independent measure of the temperature dependence of the conduction electron localization length is obtained through study of the temperature dependence of the dielectric constant. For HCl doped PAN-ES samples with weaker localization in the disordered regions, $\epsilon_{mw}(T)$ increases rapidly with increasing temperature to values in excess of 10^4 at room temperature, Fig. 34.23(c). In contrast, more localized samples have a weaker temperature dependence to the dielectric constant with ϵ_{mw} (295 K)$<2\times10^3$. Using Eq. 34.9 the room temperature localization length (L_{RT}) is estimated as ~1000 Å and ~350 Å parallel and perpendicular to the chain direction respectively for these highly conducting materials [73]. This distance encompasses of order seven or more structurally coherent regions ("crystalline islands") in the parallel direction and four or more in the perpendicular direction. Such materials were described [73] as having mesoscopic metallic states at room temperature. In contrast, for modestly conducting materials L_{RT} is less than or of order twice the distance between crystalline regions implying nearly isolated "metallic" islands.

The sign, magnitude, and temperature dependence of the 6.5×10^9 Hz dielectric constant for very highly conducting T-$[CH(I_3)_y]_x$ [75,160], PPy-PF_6 [74], and *m*-cresol prepared PAN-CSA [73] are quite striking, Fig. 34.24. For example, PAN-CSA (*m*-cresol) has a metallic negative dielectric constant and features a maximum in microwave frequency conductivity at ~180 K [73]. A similar large and negative value of ϵ_{mw} and temperature dependence of ϵ_{mw} were determined for heavily iodine doped stretched Tsukamoto polyacetylene [75,160] and PF_6 doped polypyrrole [74]. Using the Drude model [123,124] for low frequencies ($\omega\tau\ll1$), a plasma frequency of ω_p=0.015 eV (120 cm^{-1}) and a room temperature scattering time of $\tau=1.2\times10^{-11}$ sec were calculated [73] for the PAN-CSA (*m*-cresol) system, though the exact values correlate with the sample preparation. Similar values are obtained for heavily iodine doped stretched Tsukamoto polyacetylene and PF_6 doped polypyrrole (Table 34.5). These values of ω_p are much smaller than one expects from the usual Drude model. The small values of ω_p suggest that only a small fraction of the conduction band electrons participate in this low frequency plasma response. Similarly, the value of τ is two orders of magnitude larger than usual for an alkali, noble, or transition metal [124]. The origin of the anomalously large scattering time was suggested [120] to be the ineffectiveness of forward scattering of conduction electrons in the metallic state and the need for backward scattering (i.e., the Fermi surfaces of metallic polyaniline, polyacetylene, and polypyrrole are "open" as expected for highly anisotropic materials, and backward scattering from k_F to $-k_F$ may be necessary for momentum relaxation).

The behavior of ϵ_{mw} for PAN-CSA of moderate conductivity (~200 S/cm) demonstrates [120] strikingly the effect of disorder (Fig. 34.25). A metal-insulator transition as a function of temperature is reflected in ϵ_{mw}. ϵ_{mw} crosses from huge and negative (Drude-type band transport) at room temperature to large and positive (insulating or "dielectric" behavior) at ~20 K. This behavior is ascribed [120] to phonon controlled delocalization. When the

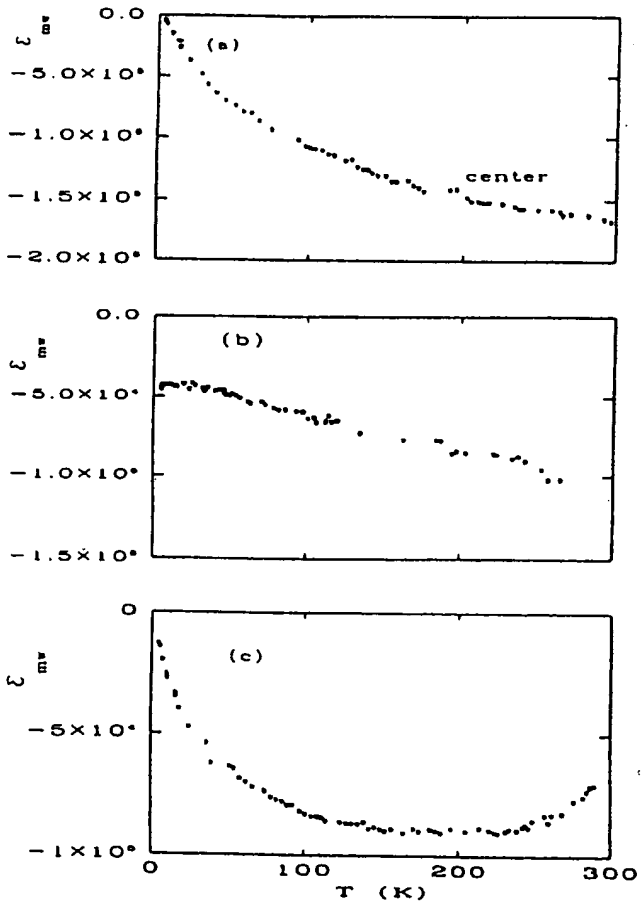

FIGURE 34.24. ϵ_{mw} (6.5×10^9 Hz) versus temperature for highly conducting doped polymers. (a) I_3 doped Tsukamoto polyacetylene (stretched central portion of sample) (from Ref. 160), (b) unstretched PPy-PF_6 (from Ref. 74), and (c) PAN-CSA (*m*-cresol) (from Ref. 73). Note the large negative values of these dielectric constants.

TABLE 34.5. *Typical low frequency plasma frequency and relaxation time obtained from microwave frequency measurements of very highly conducting polymers.*

Highly conducting polymer	ω_p (cm^{-1})	τ (sec)
T-$(CH(I_3)_y)_x$ (295 K) [75,160]	~200	$\sim 3.3\times10^{-11}$
PPy-PF_6 (265 K) [74]	~100	$\sim 3.0\times10^{-11}$
PAN-CSA (*m*-cresol) (295 K) [73,75,120]	~120	$\sim 1.2\times10^{-11}$

phonon scattering rate is larger than the impurity scattering rate, phonon scattering destroys the localization caused by impurity scattering. The presence of this effect is suggested to arise from the key role of one-dimensional chains electronically linking three-dimensional metallic regions in the polymer.

34.8 OPTICAL ABSORPTION, TRANSMISSION, AND REFLECTION

The apparent semiconducting or insulating bandgaps for each of the principal conducting polymers as obtained by visible/UV spectroscopy are listed in Table 34.6 [91,161–181], though for many of the nondegenerate polymers, the lowest energy optical absorption may actually represent formation of excitons [49–51,182–184]. Upon low level doping, there is a systematic change in the optical properties depending on whether the ground state is degenerate or nondegenerate, with prominent signatures for solitons, polarons, and bipolarons. However, for the most highly doped ordered states, the conducting polymers show "metallic" absorption and reflection behavior.

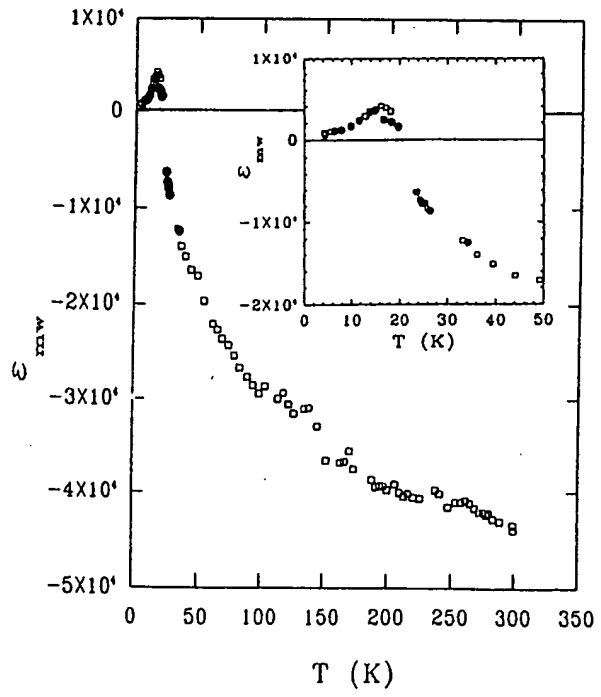

FIGURE 34.25. ϵ_{mw} (6.5×10^9 Hz) versus temperature for a sample of PAN-CSA (*m*-cresol) of moderate conductivity (~200S/cm), demonstrating a metal-insulator transition as a function of temperature (from Ref. 120).

Because the metallic state is so highly reflecting, it is often studied via reflectance from films. From such data, a Kramers-Kronig analysis provides all the optical constants of interest including the absorption coefficient, dielectric functions, and conductivity [185]. The real part of the dielectric function (ϵ_1) and the optical conductivity (σ_1) give insight into the localized or delocalized behavior of the conduction electrons. The measured frequency response can be compared with the Drude model for free electrons and other models for localized (bound) electrons [185]. Again, the universality of the electronic behavior of the systems with improving structural order, morphology, and doping is stressed. For the materials with the highest σ_{DC}, an increasing fraction of the total oscillator strength (from conduction electrons) demonstrates free electron Drude response.

34.8.1 Optical Dielectric Function

For the conducting forms of doped polyacetylene and other conducting polymers, there are zero, two, three, or one zero crossings of the real part of the dielectric function (ϵ_1) as the frequency is decreased. For the least conducting materials, ϵ_1 remains positive for the entire optical frequency range (50–50 000 cm^{-1}), reaching values of several hundred at microwave frequencies. For higher conductivity materials, ϵ_1 crosses zero between 1 and 3 eV

TABLE 34.6. *Typical apparent "bandgap" values for the undoped conducting polymers. Both the absorption onset and peak are given.*

Material	Absorption onset (eV)	Absorption peak (eV)
$(CH)_x$ (*trans*) [161,162]	1.4	1.8
$(CH)_x$ (*cis*) [163]	~1.9	2.3
PAN (LEB) [164]	3.2	3.6
PAN (EB) [164]	1.6(3.0)	2.0(3.8)
PAN (PNB) [165]	1.8	2.3
PPy [166,167]	2.5	3.2
PT [168–171]	2.0	2.3–2.7
PPP [91,172–174]	3.1	3.43–3.7
PPV (old) [175–178]	2.4	2.9
PPV (new) [179]	2.25	2.46
PPyr [180]	2.9	3.3
PPyV [181]	2.5	3.0

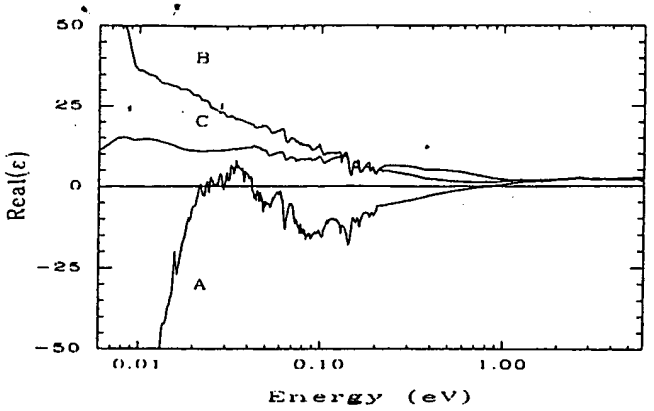

FIGURE 34.26. Real part of the room temperature dielectric response versus frequency for PAN-CSA(*m*-cresol) (A), PAN-CSA(chloroform/*m*-cresol) (B), and PAN-HCl IXL (C) (from Ref. 192,193).

(the all-conduction-electron plasma response) and then becomes positive again below 1000 cm^{-1}, reaching values in excess of 10^4 at microwave frequencies. For the most metallic samples, two behaviors have been reported dependent upon the system. For doped PAN and PPy with modest σ_{DC}~400 S/cm, ϵ_1 demonstrates the previous two zero crossings, and a third zero crossing occurs to negative values at a "delocalized conduction electron plasma frequency" of several hundred wavenumbers. For the most highly conducting doped polyacetylene, ϵ_1 crosses zero at the all conduction plasma frequency and remains negative to the lowest measured optical frequencies.

The optical response of iodine [83,106,162,186,187] and perchlorate (ClO_4) [106,188,189] doped $(CH)_x$ and PF_6 doped poly(methylthiophene) [190] have been well characterized, as have polyaniline samples (PAN-HCl [55,191,192] and PAN-CSA prepared in *m*-cresol [75,134,193–196] and in solutions of *m*-cresol and chloroform [193,197]) and polypyrrole films (doped with PF_6 [74,89,198,199], TsO [74,89,198], ClO_4 [166], and some

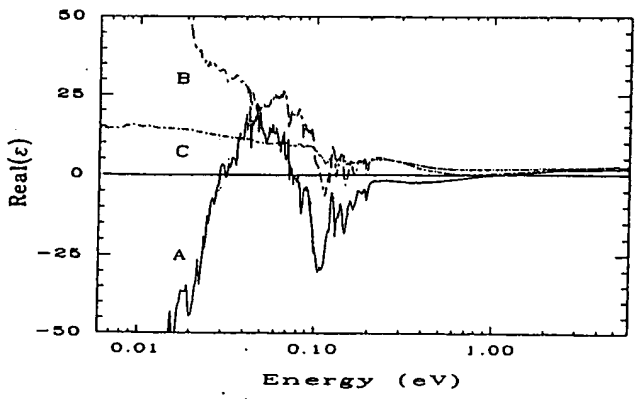

FIGURE 34.27. Real part of the room temperature dielectric response (ϵ_1) vs. frequency for PPY(PF_6) (A), PPY(TsO) (B), and PPY(S-PHE) (C) (from Refs. 74 and 192).

sulfated poly(β-hydroxyethers) [34,192]).

Fig. 34.26 shows ϵ_1 at room temperature for selected PAN samples. PAN-CSA (*m*-cresol) (σ_{DC}~400 S/cm) has three zero crossings for ϵ_1 which correspond to two different plasma frequencies [193]. The higher energy zero crossing was assigned [75] to the plasma response of the whole conduction band, as the density of carriers (n), determined from the plasma frequency ($\omega_p^2 = 4\pi ne^2/m^*$; assuming m^*, the effective mass, is approximately the free electron mass) is in the range of the dopant density. There is Lorentzian frequency dispersion at this ω_p indicating that the majority of the conduction electrons are localized or bound spatially, and require a finite amount of energy to be excited. At a lower frequency, ϵ_1 begins to become positive at ~330 cm^{-1} (~0.04 eV); this is a characteristic of the Lorentzian (localized) behavior. However, at ~200 cm^{-1} (~0.02 eV), ϵ_1 again crosses to negative values and grows increasingly negative with decreasing wavenumber. This plasma frequency shows Drude behavior with decreasing wavenumber and in fact appears approximately at the frequency predicted by the microwave estimates [73,75]. Similar zero crossings are reported for PPy(PF_6) (σ_{DC}~300S/cm) [74,198,199] (Fig. 34.27).

Comparison of the plasma frequencies for the Drude electrons with the plasma frequencies for the whole conduction band for these polymers, assuming that the effective mass m^* is the same as that for the whole conduction band response, yields a ratio of the density of electrons contributing to the free response compared to the localized response of $\sim 10^{-3}$. Assuming even a tenfold increase in m^* for the lower frequency ω_p (as the delocalized electrons must traverse the disordered regions with presumably narrowed energy bands), only a small fraction ($\sim 10^{-2}$) of the conduction electrons are delocalized enough to show Drude behavior in PAN-CSA (*m*-cresol).

The frequency response of ϵ_1 for PAN-CSA prepared from chloroform and subsequently briefly exposed to *m*-cresol vapor (σ_{DC}~20 S/cm) [193] (Fig. 34.26) is characteristic of localized electrons. ϵ_1 is positive at all optical frequencies; the scattering due to disorder in these materials has broadened and washed out the dielectric zero crossings. Lorentzian dispersion due to a "localized polaron" [134] is evident in ϵ_1 around 12 000 cm^{-1} (1.5 eV) and ϵ_1 for this material increases positively with decreasing wavenumber in the far IR, characteristic of a material with a small residual band gap or localized carriers. Lower conductivity PAN-HCl [193] (σ_{DC}~10 S/cm) materials show even less dispersion with wavenumber. ϵ_1 for these materials is also positive over the whole range and shows only a modest increase in the IR, becoming nearly wavelength independent in the far IR.

Polarized optical measurements of the dielectric response of HCl doped stretched PAN samples are shown in Fig. 34.28. The dielectric response perpendicular to the stretch direction is characteristic of insulating behavior. Along the stretch direction, a strong plasma-like response is observed

[191], indicating that the scattering times along the chain are much longer than those perpendicular to the chain. This indicates that on-chain partial delocalization develops first in these systems.

Doped polypyrrole demonstrates behavior similar to polyaniline for samples with lower conductivity and structural order. In Fig. 34.27, the more disordered PPy(TsO) (σ_{DC}~120 S/cm) [74,198] shows a more localized behavior than PPy(PF_6) as ϵ_1 remains positive throughout the optical frequency range. The carriers are weakly localized though as ϵ_1 increases rapidly in the far IR. For PPy(S-PHE) (σ_{DC}~10 S/cm) [34,192], there is very little dispersion in ϵ_1; it remains positive and small in the entire optical range, becoming nearly wavelength independent in the far IR.

ϵ_1 for the most highly conducting iodine and perchlorate doped polyacetylene samples remains negative but small for frequencies less than its all-conduction-electron plasma frequency of ~3 eV through the far IR for light polarized both parallel and perpendicular to the stretched chain direction [187,188] (Fig. 34.29) again supporting the three-dimensional nature of the metallic state in conducting polymer systems. Below ~0.05 eV, ϵ_1 becomes increasingly negative, suggesting a Drudè plasma frequency for the most delocalized electrons.

Summarizing, there is an evolution of the dielectric response with increasing order. For the most disordered, lowest conducting samples, ϵ_1 remains positive and shows very weak dispersion. As the order and conductivity of the materials increase, ϵ_1 first shows more dispersion at the plasma edge of the whole conduction band as the scattering time increases, possibly turning negative in that range, but returns positive in the far IR. This behavior was seen in stretched PAN- HCl samples parallel to the stretch direction [191]. For the best current materials, ϵ either returns negative or remains negative in the far IR, indicative of a small density of macroscopically delocalized electrons.

34.8.2 Optical Conductivity

For materials near the insulator-metal (localization-delocalization) transition the optical conductivity is suppressed

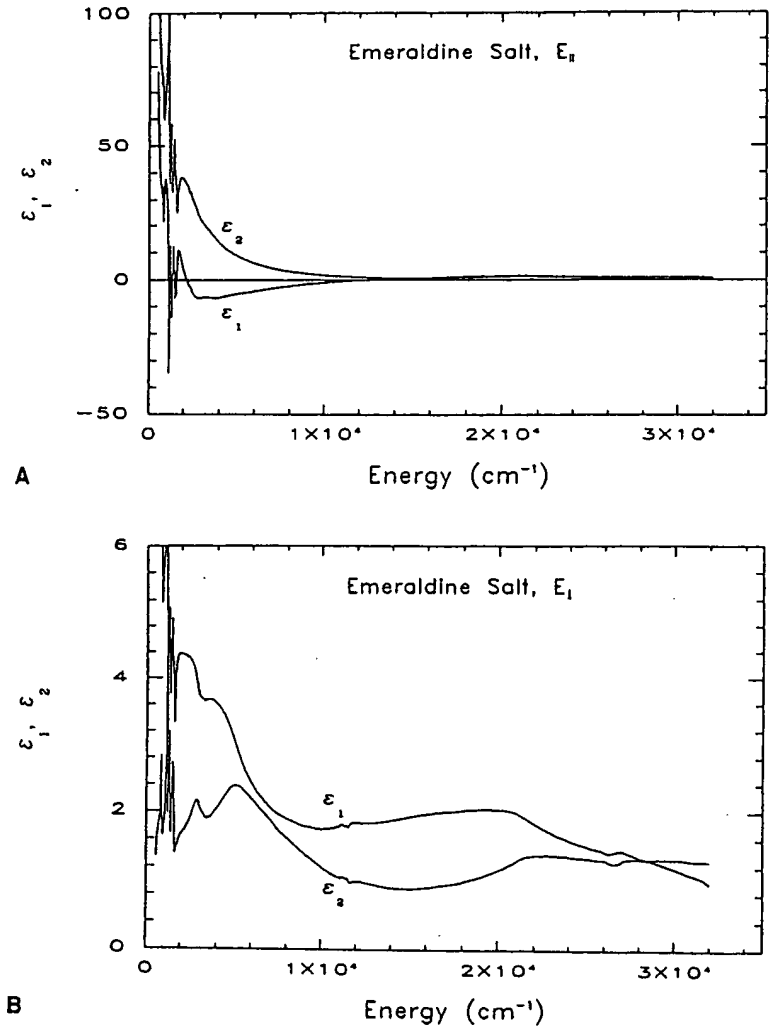

FIGURE 34.28. Real part of the dielectric constant vs. frequency for light polarized (**A**) parallel and (**B**) perpendicular to the stretch direction in PAN doped with HCl (from Ref. 191). The chain alignment is improved by stretching. ϵ_1 is negative in the mid IR for the parallel direction but not for the perpendicular direction, implying that the delocalization is much greater along the chain.

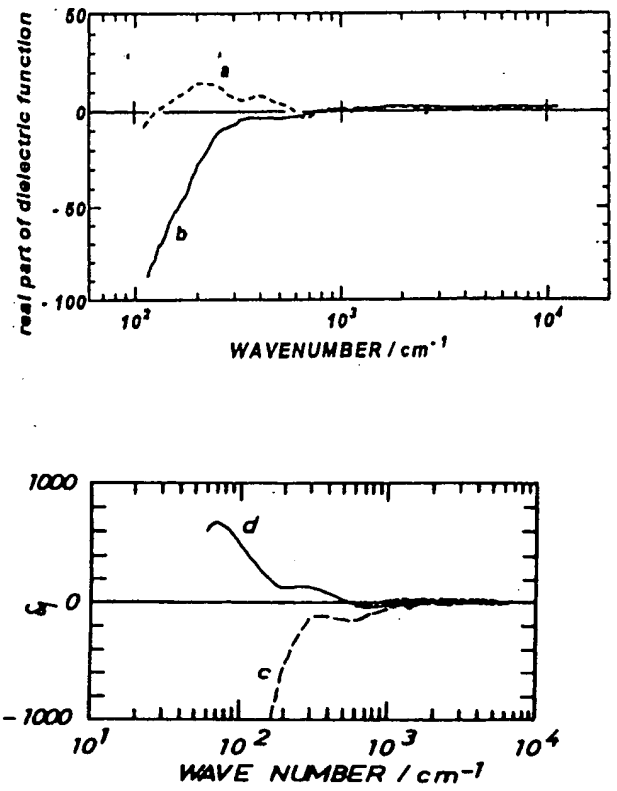

FIGURE 34.29. Top: real part of the dielectric constant vs. frequency for light polarized perpendicular to the stretch direction in $(CH)_x$ doped with ClO_4 (from Ref. 188). For sample (b), the chain alignment is improved over sample (a) by stretching. ϵ_1 is negative at low frequencies indicating a three-dimensional metallic state. Bottom: real part of the dielectric constant vs. frequency for light polarized parallel to the stretch direction (from Ref. 187). Samples (c) and (d) are both doped to the same level with iodine, but sample (c) was stretched before doping, resulting in greater ordering and a more metallic response.

at low frequencies relative to the usual Drude conductivity [115]. The suppression is usually strong for frequencies up to a critical frequency $\omega_c \sim D/L^2$ where D is the diffusion coefficient and L is the localization length for the electron. This conductivity suppression occurs because the carriers would diffuse a distance greater than the localization length within the period of the AC wave for $\omega < \omega_c$. For frequencies greater than ω_c, the optical conductivity shows the normal Drude decrease with increasing frequency. For three-dimensional materials, localization corrections to the frequency dependent conductivity [115,194,200–202] yield

$$\sigma(\omega) = \sigma_{\text{Drude}}\left[1 - \frac{C}{(k_F v_F \tau)^2} + \frac{C(3\omega)^{1/2}}{(k_F v_F)^2 \tau^{3/2}}\right], \tag{34.10}$$

where C is an undetermined universal constant, k_F is the Fermi wavevector, v_F is the Fermi velocity, τ is the scattering time, and σ_{Drude} is the regular Drude conductivity given by

$$\sigma_{\text{Drude}} = \frac{\Omega_p^2 \tau}{4\pi(1+\omega^2\tau^2)}, \tag{34.11}$$

where Ω_p is the plasma frequency of the free electrons. Notice that as $k_F l$ (i.e., $k_F v_F \tau$) becomes large for more ordered higher σ materials, the corrections to the Drude formula should become negligible and the three-dimensional conductor should obey the Drude formula.

The experimental optical conductivity of the doped polymers evolves from localized semiconducting behavior to metallic behavior with improved order. For $(CH)_x$ doped with perchlorate (ClO_4) [106,188,189], (Fig. 34.30) or iodine [106,162,186] with different stretch ratios, the optical conductivity shows soliton features at midgap and a Drude plasma edge which develops with stretch alignment at ~200 cm^{-1} (0.02 eV) where the optical conductivity rises rapidly to its dc value with a very long scattering time. The full conduction electron plasma frequency for doped $(CH)_x$ is ~3 eV; therefore, the plasma edge at 0.02 eV is associated with only a small fraction of the conduction electrons [75]. Because a small fraction of the conduction electrons appear macrocroscopically delocalized with a long scattering time while the majority of conduction electrons are more strongly localized, with a short scattering time, the localization modified Drude model [115,194,200–202] does not simultaneously fit well the frequency dependent dielectric function and conductivity of highly conducting $(CH)_x$. Models which take into account the inhomogeneous disorder of the systems provide a better representation as they allow for composite behavior (metallic islands which percolate in a semiconducting matrix.)

Typical optical conductivity spectra for PAN and PPy films are shown in Figs. 34.31 and 34.32, respectively. For highly conducting PAN-CSA (m-cresol) [σ_{DC}=400 S/cm]

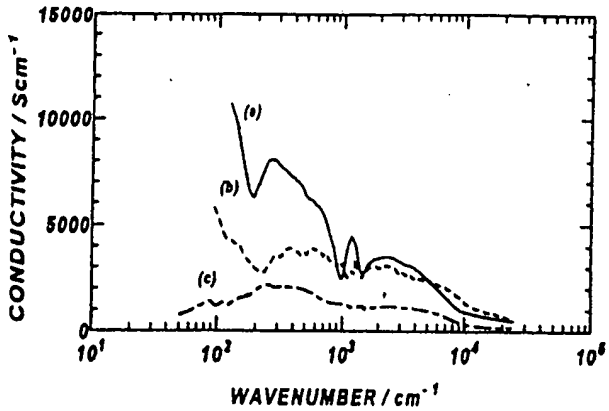

FIGURE 34.30. Optical conductivity vs. frequency for $(CH)_x$ of different stretch ratios (a: stretched 8×; b: stretched 4×; c: unstretched) doped with perchlorate (ClO_4) (from Ref. 188). There is a growth of a free carrier band (Drude response) around ~200 cm^{-1} with increased stretch ratio.

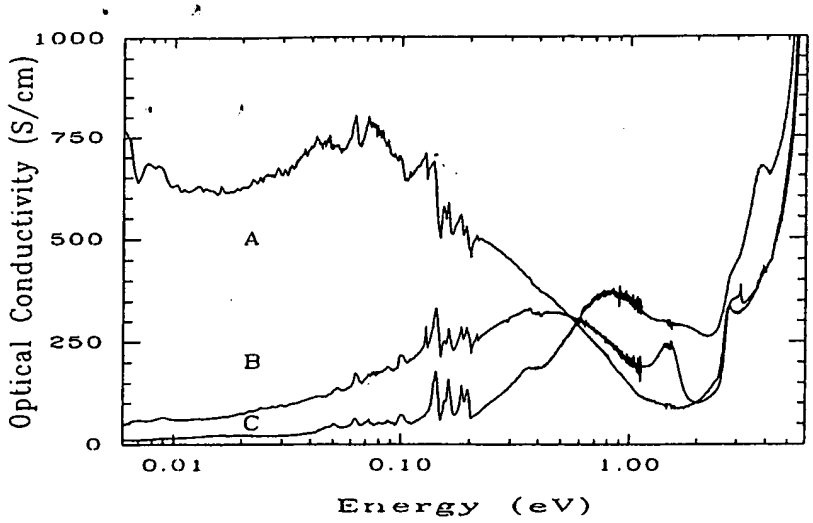

FIGURE 34.31. Room temperature optical conductivity vs. frequecy for PAN-CSA(*m*-cresol) (A), PAN-CSA (chloroform/*m*-cresol) (B), and PAN-HCl IXL (C) (from Refs. 192 and 193).

[193], σ_1 begins to increase with decreasing wavenumber at ~10 000 cm^{-1} (~1.2 eV) to values as high as ~750 S/cm at ~0.1 eV and then decreases consistent with localization behavior. However, at ~0.02 eV, σ_1 begins to increase, qualitatively similar to the behavior of doped $(CH)_x$ though the increase in the far IR is not as rapid as for doped $(CH)_x$ as the dc conductivity is much lower for this PAN-CSA material. This type of frequency behavior for σ_1 is qualitatively similar to the composite behavior of metallic particles (islands) in a semiconducting matrix after percolation of the metallic particles [203]. PPy(PF_6) [74,198] [$\sigma_{DC} \approx 300$ S/cm] has similar behavior, though σ begins to increase with decreasing wavenumber at a higher all-conduction-electron "plasma edge" of ~17,000 cm^{-1} (~2.1 eV)

In contrast to this behavior, σ for other doped PAN and PPy materials show more localized behavior. For example, the optical conductivity of PAN-CSA cast from a solution of chloroform and exposed to *m*-cresol [σ_{DC}=20 S/cm] [192], PAN-HCl ("intermediate cross linked (crystallinity)" IXL) [σ_{DC}~10 S/cm] [193], PPy(TsO) [74,198] [$\sigma_{DC} \approx 100$ S/cm], and PPy(S-PHE) [$\sigma_{DC} \approx 10$ S/cm] [34,192] have maxima (in addition to phonon features) at higher energies in the IR than more highly conducting PAN and PPy. In the far IR, σ decreases with decreasing frequency more rapidly for these samples with increased disorder as expected for localized electrons. Similar behavior has been reported for perchlorate (ClO_4) doped PPy [166,187] and PF_6 doped poly(3-methylthiophene) [190] (Fig. 34.33). For the lower conductivity doped polymers, the localization modified Drude model [115,200–202] has the same frequency dependence as the experimental spectra. The low frequency conductivity peak shifts to lower energy with increasing dc conductivity in both PAN [197] (Fig. 34.31) and PPy [74] (Fig. 34.32) and likely results from the decrease of the critical frequency ω_c as the samples become more ordered. For the low conductivity PAN samples, most of the oscillator strength is shifted [134] into a peak at ~1.5 eV associated [54,134] with localized polarons. Thus with decreasing order the oscillator strength shifts to higher wavenumber and thus higher binding energies.

Qualitatively, the PAN and PPy materials with σ_{DC}<200 S/cm show the behavior expected for both the good

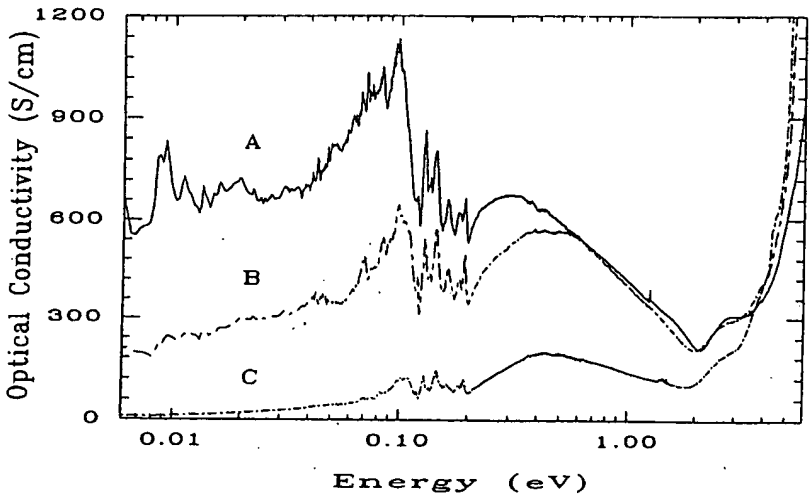

FIGURE 34.32. Room temperature optical conductivity vs. frequency for PPy(PF_6) (A), PPy(TsO) (B), and PPy(S-PHE) (C) (from Refs. 74 and 192).

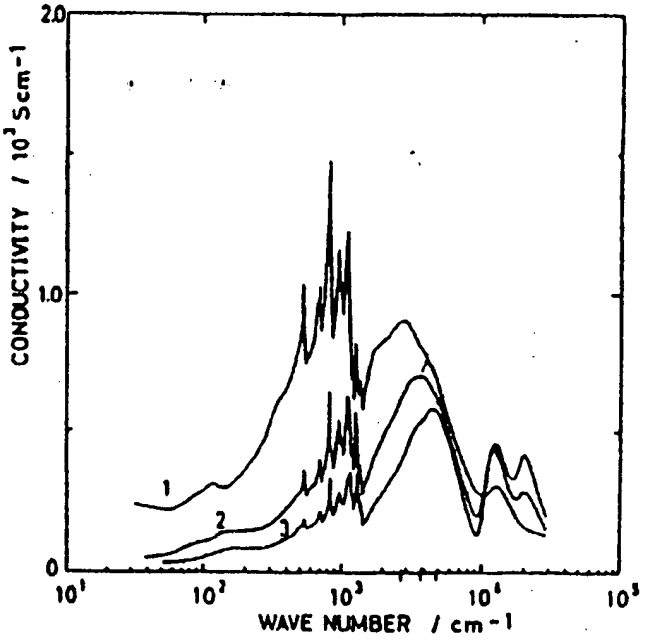

FIGURE 34.33. Optical conductivity vs. frequency for poly-(methylthiophene) (PMT) doped with PF_6 as a function of doping level (from Ref. 190). The spectra are for different doping levels [with (1) being highest and (3) the lowest doping level].

conductor/poor conductor composites as well as for the three-dimensional localization modified Drude model. The optical conductivity of highly conducting stretched polyacetylene and doped PAN and PPy with $\sigma_{DC}>200$ S/cm show Drude behavior for a small fraction of the conduction electrons which essentially percolate through the film while the remaining conduction electrons are more localized.

34.9 ULTIMATE CONDUCTIVITY

The intrinsic conductivity of conducting polymers is of interest for fundamental science and future materials applications. Though the materials currently have σ_{DC} less than common metals, the conducting polymers are not fully crystalline. Past progress suggests that as the synthesis, doping routes, and processing are improved, further advances in materials properties can be expected. Estimates of the ultimate conductivity [122] of the quasi-one-dimensional polymer systems assuming the primary momentum relaxations are from $2k_F$ phonons which have modest population at room temperature suggests the ultimate conductivity for $(CH)_x$ is $\sim 2\times10^6$ S/cm (compared to 5.5×10^5 S/cm for copper).

From the experimental data which exist for current systems, estimates of the intrinsic conductivity also can be made [197]. The intrinsic Drude nature of metallic carriers has been identified using both microwave and optical techniques. Both of these techniques have identified the presence of a group of carriers which demonstrate Drude behavior with a long scattering time ($\tau\sim10^{-11}$ s). The Drude conductivity for traditional metals is given by $\sigma=ne^2\tau/m^*$. In the present systems, only a small fraction of the conduction electrons show this Drude behavior. If all of the conduction electrons (determined by doping percentage) have a scattering time equivalent to $\tau\sim10^{-11}$ s, then $\sigma_{\text{ultimate}}\sim10^7$ S/cm.

34.10 APPLICATIONS

Intrinsically conducting polymers (ICPs) also are of interest for a wide range of applications [204]. The ICPs have been proposed for use as conducting wires, in batteries [205], as electromagnetic interference (EMI) shielding materials [206–209], joining (welding) of plastic materials

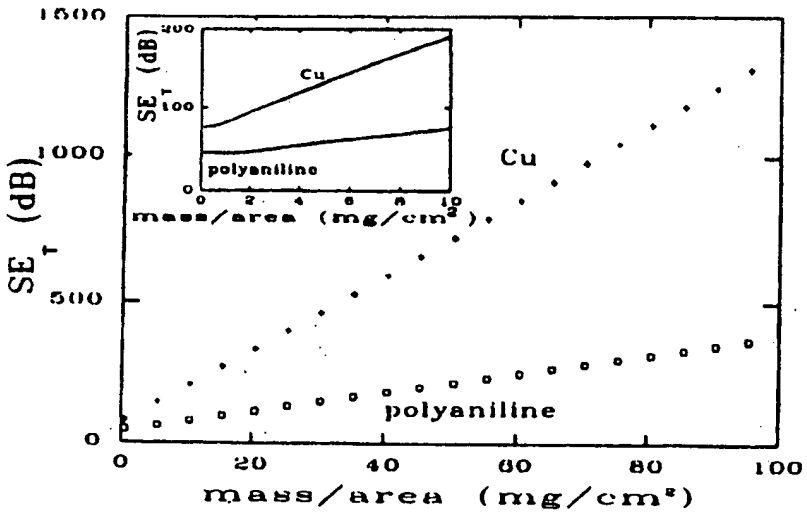

FIGURE 34.34. Comparison of total shielding efficiency (SE_T) of PAN-CSA (*m*-cresol) samples and copper (Cu) as a function of mass/area. Inset: magnification below 10 mg/cm^2 (from Ref. 207).

[210], light emitting diodes (LEDs) [211], sensors [212], anticorrosive coatings [213], etc.

In LED studies, doped polyaniline and its blends have been used for the hole injecting layer [214], and undoped poly (*p*-phenylene vinylene) and other materials have been utilized for the light emitting layer [211]. More recently, a symmetrically configured alternating voltage light emitting (SCALE) device based on electronic polymers has been demonstrated [215]. The advantages of ICPs for light emitting devices include flexibility, mechanical strength, and relatively easy control of the color of light emission. Transparent conducting polymers may be incorporated as electrodes into efficient LEDs [216].

The use of plastics and their composites is rapidly increasing in numerous areas. However, the final assembly of products is often limited by the capability of existing joining techniques. The ability of ICPs, especially polyanilines, to absorb electromagnetic radiation and convert it into heat introduces another application in the welding of thermoplastics and thermosets [210].

With the rapid advances and broad implementation of computer and telecommunication technologies there is an increased need to shield EMI, especially in the radio and microwave frequency ranges. Intrinsically conducting polymers are promising materials for shielding of EMI because of their relatively high conductivity and dielectric constant and the ease of control of their conductivity and dielectric constant through chemical processing [207]. Also, they are relatively lightweight compared to standard metals, flexible, and do not corrode as common metals. The microwave conductivity and dielectric constant of polyanilines are controllable through chemical processing (e.g., stretch ratio, molecular weight, doping level, counter ion, solvent, etc). Figure 34.34 compares the total shielding efficiency of PAN-CSA (*m*-cresol) materials with that of copper on the base of mass/area, while Fig. 34.35 compares the shielding efficiency of several different conducting polymer systems.

The ability to disperse conducting polymers into insulating hosts such as poly(3-octylthiophene) in polyethylene [217] and PAN-CSA in polymethylmethacrylate [218], or nylon [219], and achieve percolation at less than one percent, increases opportunities for applications.

34.11 SUMMARY

The electrical transport properties of conducting polymers span the behaviors associated with semiconductors through to metals. Their properties depend critically upon the history of chemical synthesis, processing, and resulting structural order. Highly conducting doped polyacetylene, doped polypyrrole, and protonated polyaniline have similar dielectric responses, though on somewhat different scales. For each of these systems a positive dielectric constant is recorded at microwave frequencies for less conducting samples. A complex "metallic Drude response," involving both an all conduction band electron response and a delocalized electron response, is detected for well processed, highly conducting samples. The ability to engineer the electrical and dielectric properties using chemistry opens the opportunity for a wide range of applications.

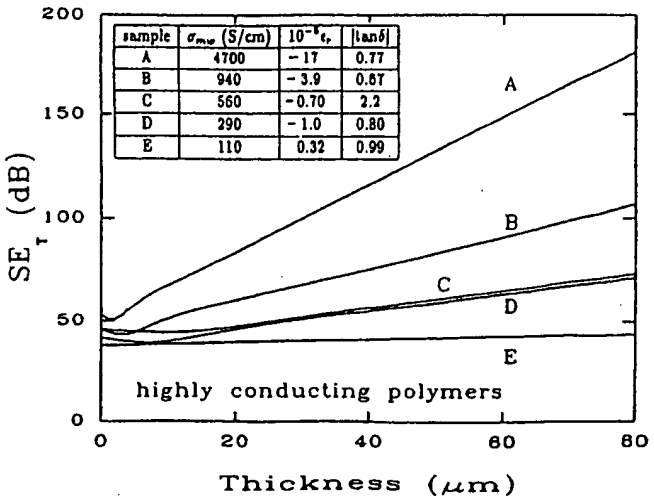

FIGURE 34.35. Comparison of the total shielding efficiency (SE_T) of highly conducting polymers versus sample thickness. Sample A: stretched heavily iodine doped Tsukamoto polyacetylene; sample B: unstretched heavily iodine doped Tsukamoto polyacetylene; sample C: PAN-CSA (*m*-cresol); sample D: $PPy(PF_6)$; sample E: PPy(TsO) (from Ref. 207). The inset shos the microwave transport parameters σ_{mw}, ϵ_r, and $\tan\delta$ for each of the materials.

ACKNOWLEDGMENTS

This work was supported in part by the Office of Naval Research and by National Institute for Science and Technology.

GLOSSARY OF TERMS

Anderson Localization: spatial localization of electronic wavefunctions due to randomness of the electronic potential which causes a metal-insulator transition in sufficiently disordered materials.

Anti-Soliton: solitons are present in materials with two degenerate phases A and B. If a soliton is a kink between A and B phase, then an anti-soliton is a kink between B and A phase.

Bipolaron: a bipolaron is similar to a polaron except that it is doubly charged, spinless and both of its energy states in the band gap are totally filled or empty.

Bloch Waves: Delocalized electronic wavefunctions which have the form $\psi_k(\vec{r}) = u_k(\vec{r})exp(i\vec{k}\cdot\vec{r})$, where $u_k(\vec{r})$ is a function with the periodicity of the lattice unit cell and $exp(i\vec{k}\cdot\vec{r})$ is a wave of wavelength $\lambda = 2\pi/k$.

Commensurate Charge Density Wave: a static modulation of the charge density in the system with a periodicity

equal to a rational number multiplied by the underlying periodicity of the lattice. Due to the charge density wave, a gap is opened at the Fermi level which lowers the total energy of the system.

Crosslinked Polymers: polymers with greater interaction between chains either through regions of greater crystallinity (physical crosslinks between the polymer chains), or through chemical bonding between chains.

Crystalline Coherence Length: a length which characterizes the spatial correlations for the polymer chain, indicating the length over which the local order randomizes. This length is determined from the width of x-ray scattering peaks from the Scherrer formula.

Curie Susceptibility: Paramagnetic susceptibility due to uncoupled spins free to align in a magnetic field and subject only to thermal fluctuations. The Curie susceptibility is given by $\chi_{\text{Curie}}=C/T$, where C is the Curie constant (0.375 emu-K/mol) and T is the temperature.

Degenerate Ground State: for a degenerate ground state, the conjugation path is such that reversal of the single and double bonds results in a phase of the system with an equivalent energy.

Doping: a process whereby charges are removed or added to the polymer chain, altering the electronic structure and response.

Drüde Model: this model of the electrons in a conductor treats the electrons as free, subject only to dissipative, inertial, and electromagnetic forces. In this model, the conductivity $\sigma(\omega)$ and the dielectric function $\epsilon(\omega)$ are given as $\sigma(\omega)=(\Omega_p^2\tau/4\pi)/(1-i\omega\tau)$ and $\epsilon(\omega)=\epsilon_B-\Omega_p^2/(\omega(\omega+i/\tau))$, where Ω_p is the plasma frequency and τ is the mean scattering for transport.

Electron-Electron Interactions: a broad term referring to the electromagnetic interaction between electrons as well as some of the effects of the the Pauli exclusion principle.

Exciton: an electron-hole pair bound by Coulombic forces capable of transferring energy but not charge because it is electrically neutral.

Hole: a vacant orbital in an energy band which acts as a positive charge in an applied electric or magnetic field.

Hopping Transport: a form of charge transport which involves electron motion from one spatially localized state to another accompanied by the absorption or emission of a phonon.

Incommensurate Charge Density Wave: similar to a commensurate charge density wave except that the periodicity of the charge density modulation does not equal a rational number multiplied by the periodicity of the underlying lattice.

Inhomogeneous Disorder: structural configuration for a polymer solid which consists of a mixture of ordered (crystalline) and disordered regions of the polymer.

Kramers-Kronig Analysis: a set of mathematical relations due to causality which relate the real (dispersive) and imaginary (absorptive) parts of a physical quantity. These relations can be used to determine the imaginary part of a quantity given information about the real part and vice versa.

Localization Modified Drude Model: a model for conduction electrons which includes suppression of the Drude conductivity at low frequencies due to finite localization lengths for the electrons.

Localized States: electronic states which are not extended over the entire solid as Bloch waves are. The spatial dependence of the wavefunction of a localized state is usually assumed to vary as $|\psi(\vec{r})|\sim\exp(-|\vec{r}-\vec{r}_0|/\xi)$, decaying exponentially in a characteristic length ξ, the localization length, away from $\vec{r}_0$. Charge transport by electrons in these states is due to hopping.

Lorentz Model: this model treats electrons as bound strongly to an atom, subject to dissipative, inertial, electromagnetic, as well as restoring forces. In this model, the dielectric function $\epsilon(\omega)$ is given by $\epsilon(\omega)=\epsilon_B+\Omega_p^2/(\omega_0^2-\omega^2-i\omega/\tau)$, where ϵ_B is the background dielectric function due to everything else, Ω_p is the plasma frequency, ω_0 is the binding energy, and τ is the mean scattering time.

Mesoscopic Metallic State: a metallic state in an inhomogeneous system in which conduction electrons are delocalized over a number of crystalline regions (with disordered polymer regions between them). The size of the localization length is $\sim 10^2-10^3$ Å, smaller than macroscopic dimensions (10^4 Å or greater).

Mobility Edge: the critical energy which separates electronic states which are spatially localized due to disorder and thus have zero contribution to the electrical conductivity at very low temperature from those which are delocalized and therefore have non-zero contribution to the electrical conductivity at low temperature.

Mott Variable Range Hopping: a form of hopping transport which results when the electron may hop to a distant site instead of just a neighboring site if the energy difference between its current site and the distant site is smaller than the difference between its current site and the neighboring sites. Mott Variable Range Conductivity has a form given by $\sigma(T)=\sigma_0\exp[-(T_0/T)^{1/(d+1)}]$, where d is the dimensionality of the hops and T_0 is a reduced activation energy.

Nondegenerate Ground State: for a nondegenerate ground state, the conjugation path is such that reversal of the single and double bonds results in a distinctly different energy.

One-Dimensional Chain: a linear system for which the interactions along the chain direction are much stronger than the interactions perpendicular to the chain.

p_z Orbitals: electron wavefunctions with atomic principal quantum number p character which have a node in the x-y plane (the x-y plane is usually taken as the plane of the polymer sp^3 bonds.) Electrons in these orbitals usually pair to form double bonds and provide the conjugation responsible for the interesting electronic properties of conducting polymers.

π Conjugation: alternating single and double bonds in a single plane due to the overlap of atomic p_z orbitals along the polymer backbone. π conjugation leads to the electronic bands responsible for the interesting electronic properties of conducting polymers.

Pauli Susceptibility: paramagnetic, approximately temperature independent magnetic susceptibility due to conduction electrons. The Pauli susceptibility, $\chi_{\text{Pauli}}=2\mu_B^2 N(E_F)$, where μ_B is a Bohr magneton and $N(E_F)$ is the density of states at the Fermi level.

Peierls Instability: an instability prominent in quasi-one-dimensional systems with strong electron-phonon interactions due to which the lattice spontaneously distorts with a $2k_F$ (k_F is the Fermi wavevector) periodicity, forming a gap at the Fermi level which lowers the total energy of the system.

Percolation: in a solid made up of more than one component (a composite system), the volume fraction of the different components can be varied. Percolation refers to the transitions which occur when the volume fraction of a component is such that there are connected paths of that component across the material. For example, in a composite of a metal and an insulator, the metal particles percolate when they form a connected path across the material and finite dc conductivity becomes possible.

Phonon: a quantum of lattice vibrational energy which reflects the normal vibrational modes of the lattice allowed by symmetry.

Phonon Induced Delocalization: in disordered solids, localization can result when a wavefunction interferes with itself due to elastic scattering and forms a standing wave. Phonon scattering can destroy this interference effect and cause the wavefunctions to be more extended.

Photoexcitation: the use of light (photons) to cause transitions of electrons from the ground state to excited states of the system.

Plasma Frequency: defined as $\Omega_p=4\pi ne^2/m^*$, where n is the volume density of conduction electrons, e is the charge of an electron, and m^* is the effective mass renormalized from the free electron mass by lattice and interaction effects.

Plasma Response: an excitation of a solid for which the negative charge in the solid is displaced uniformly with respect to the ions. Plasma oscillations occur when the dielectric function is equal to zero.

Polaron: most generally a localized electronic state accompanied by a surrounding lattice distortion. In conducting polymers, it has been discussed as a bound state of a soliton and an antisoliton. This excitation can occur in degenerate and non-degenerate ground state polymers. A polaron possesses a single charge with normal spin-charge relations (i.e., with a single charge, it also has spin 1/2) and usually two states in the bandgap of the neutral polymer, one of which is half filled.

Polaron Lattice: a uniform periodic array of "polarons" assumed stabilized against a Peierls distortion by interchain interaction. The band structure for a polaron lattice is metallic.

Screened Plasma Frequency: the plasma frequency normalized or screened by a background dielectric constant. The screened plasma frequency, $\omega_p=\Omega_p/\sqrt{\epsilon_B}$, where Ω_p is the plasma frequency and ϵ_B is the background dielectric constant due to all excitations except the conduction electrons.

Soliton: a low energy excitation of the electronic system which is localized in space and maintains its identity in the presence of other excitations. In conducting polymers, a soliton takes the form of a kink or misfit between two distinct energetically equivalent phases (in degenerate ground state systems). Its properties include a reversed spin-charge relation (i.e., when it is charge neutral, it has spin 1/2), the introduction of a single energy level within the band gap of the polymer, and a lattice distortion surrounding the soliton.

Time Reversal Symmetry: a symmetry of a system characterized by replacing t (time) with $-t$ without changing the physics of the system.

REFERENCES

For a more complete set of annotated references, see J. W. Blatchford and A. J. Epstein, Am. J. Phys. **64**, 120–135 (1996); for a compilation of original papers, see YU Lu, *Solitons & Polarons in Conducting Polymers* (World Scientific, New Jersey 1988).

1. See Chapters 35, 37, and 38 of this handbook.
2. C. K. Chiang, C. R. Fincher, Jr., Y. W. Park, A. J. Heeger, H. Shirakawa, E. J. Louis, S. C. Gau, and A. G. MacDiarmid, Phys. Rev. Lett. **39**, 1098 (1977).
3. Proc. Int. Conf. on Science and Technology of Synthetic Metals, ICSM-'94, Seoul, Korea, July 21-29, 1994, in Synth. Met. **69-71** (1995); ICSM '92, Goteborg, Sweden, Aug. 12-18, 1992, in Synth. Met. **55-57** (1993); ICSM '90, Tubingen, FRG, Sept. 2-9, 1990, in Synth. Met. **41-43** (1991); and ICSM '88, Santa Fe, NM, June 26- July 2, 1988, in Synth. Met. **27-29** (1988).
4. *Handbook of Conducting Polymers*, edited by T. A. Skotheim (Marcel Dekker, New York, 1986).
5. D. Baeriswyl, D. K. Campbell, and S. Mazumdar, in *Conjugated Conducting Polymers*, edited by H. G. Keiss (Springer-Verlag, Berlin, 1992), p. 7.
6. E. M. Conwell, IEEE Transactions on Electrical Insulation **EI-22**, 591 (1987).
7. A. J. Heeger, S. A. Kivelson, J. R. Schrieffer, and W. P. Su, Rev. Mod. Phys. **60**, 781 (1988).
8. E. Jeckelmann and D. Baeriswyl, Synth. Met. **65**, 211 (1994).
9. J. E. Hirsch, Phys. Rev. Lett. **51**, 296 (1983).
10. S. N. Dixit and S. Mazumdar, Phys. Rev. B **29**, 1824 (1984).
11. W. K. Wu and S. Kivelson, Phys. Rev. B **33**, 8546 (1986).
12. C. Wu, X. Sun, and K. Nasu, Phys. Rev. Lett. **59**, 831 (1987).
13. H. W. Gibson, F. C. Bailey, A. J. Epstein, H. Rommelmann, S. Kaplan, J. Harbour, X.-Q. Yang, D. B. Tanner, and J. M. Pochan, J. Am. Chem. Soc. **105**, 4417 (1983); K. Pakbaz, R. Wu, F. Wudl, and A. J. Heeger, J. Chem. Phys. **99**, 590 (1993).
14. M. C. dos Santos and J. L. Brédas, Phys. Rev. Lett. **62**, 2499 (1989).
15. J. M. Ginder and A. J. Epstein, Phys. Rev. Lett. **64**, 1184 (1990).
16. W. P. Su and A. J. Epstein, Phys. Rev. Lett. **70**, 1497 (1993).
17. J.-C. Chiang and A. G. MacDiarmid, Synth. Met. **13**, 193 (1986).
18. J. P. Pouget, Z. Oblakowski, Y. Nogami, P. A. Albouy, M. Laridjani, E. J. Oh, Y. Min, A. G. MacDiarmid, J. Tsukamuto, T. Ishiguro, and A. J. Epstein, Synth. Met. **65**, 131 (1994).

19. M. Winokur, Y. B. Moon, A. J. Heeger, J. Barker, D. C. Bott, and H. Shirakawa, Phys. Rev. Lett. 58, 2329 (1987); R. H. Baughmann, S. L. Hsu, G. P. Pez, and A. J. Signorelli, J. Chem. Phys. 68, 5405 (1978).
20. N. S. Murthy, G. G. Miller, and R. H. Baughmann, J. Chem. Phys. 89, 2523 (1988).
21. W. P. Su, J. R. Schrieffer, and A. J. Heeger, Phys. Rev. Lett. 42, 1698 (1979).
22. S. A. Brazovskii, Sov. Phys. JETP. Lett. 28, 606 (1978).
23. M. J. Rice, Phys. Lett. 71A, 152 (1979).
24. D. K. Campbell and A. R. Bishop, Phys. Rev. B 24, 4859 (1981).
25. C. R. Wu, J. O. Nilsson, O. Inganäs, W. R. Salaneck, J.-E. Österholm, and J. L. Brédas, Synth. Met. 21, 197 (1988).
26. C. X. Cui and M. Kertesz, Phys. Rev. B 40, 9661 (1989).
27. F. Moraes, D. Davidov, M. Kobayashi, T. C. Chung, J. Chen, A. J. Heeger, and F. Wudl, Synth. Met. 10, 169 (1985).
28. G. Harbeke, E. Meier, W. Kobel, M. Egli, H. Kiess, and E. Tosatti, Solid State Commun. 55, 419 (1985).
29. G. S. Kanner, X. Wei, B. C. Hess, L. R. Chen, and Z. V. Vardeny, Phys. Rev. Lett. 69, 538 (1992).
30. K. Kaneto, S. Hayashi, S. Ura, and K. Yoshino, J. Phys. Soc. Jpn. 54, 1146 (1985).
31. J. L. Brédas, J. C. Scott, K. Yakushi, and G. B. Street, Phys. Rev. B 30, 1023 (1984).
32. G. Zotti and G. Schiavon, Synth. Met. 41-43, 445 (1991).
33. F. Genoud, M. Guglielmi, M. Nechtschein, E. Genies, and M. Salmon, Phys. Rev. Lett. 55, 118 (1985).
34. O. Chauvet, S. Paschen, L. Forro, L. Zuppiroli, P. Bujard, K. Kai, and W. Wernet, Synth. Met. 63, 115 (1994).
35. P. Gomes da Costa, R. G. Dandrea, and E. M. Conwell, Phys. Rev. B 47, 1800 (1993).
36. M. Onoda, Y. Manda, T. Iwasa, H. Nakayama, K. Amakawa, and K. Yoshino, Phys. Rev. B 42, 11826 (1990).
37. A. Sakamoto, Y. Furukawa, and M. Tasumi, J. Phys. Chem. 96, 1490 (1992); *ibid*, J. Phys. Chem. 96, 3870 (1992); *ibid*, Synth. Met. 55-57, 593 (1993).
38. J. L. Brédas, R. R. Chance, and R. Sibley, Phys. Rev. B 26, 5843 (1982).
39. G. Froyer, Y. Pelous, A. Siove, F. Genoud, M. Nechtschein, and B. Villeret, Synth. Met. 33, 381 (1989).
40. Y. Furukawa, H. Ohtsuka, and M. Tasumi, Synth. Met. 55-57, 516 (1993).
41. J. Libert, J. L. Brédas, and A. J. Epstein, Phys. Rev. B 51, 5711 (1995).
42. J. M. Ginder and A. J. Epstein, Phys. Rev. B 41, 10674 (1990).
43. S. Kivelson and W. K. Wu, Phys. Rev. B 34, 5423 (1986).
44. X. Wei, B. C. Hess, Z. V. Vardeny, and F. Wudl, Phys. Rev. Lett. 68, 666 (1992).
45. S. Abe, J. Yu, and W. P. Su, Phys. Rev. B 45, 8264 (1992).
46. H. A. Mizes and E. M. Conwell, Phys. Rev. B 50, 11243 (1994).
47. M. Chandross, S. Mazumdar, S. Jeglinski, X. Wei, and Z. V. Vardeny, Phys. Rev. B 50, 14702 (1994).
48. M. J. Rice and Y. N. Gartstein, Phys. Rev. Lett. 73, 2504 (1994).
49. N. F. Colaneri, D. D. C. Bradley, R. H. Friend, P. L. Burn, A. B. Holmes, and C. W. Spangler, Phys. Rev. B 42, 11670 (1990).
50. M. Yan, L. J. Rothberg, F. Papadimitrakoupoulos, M. E. Galvin, and T. M. Miller, Phys. Rev. Lett. 72, 1104 (1994).
51. J. M. Leng, S. Jeglinski, X. Wei, R. E. Benner, Z. V. Vardeny, F. Guo, and S. Mazumdar, Phys. Rev. Lett. 72, 156 (1994).
52. E. M. Conwell, H. A. Mizes, and S. Javadev, Phys. Rev. B 40, 1630 (1989).
53. S. Stafstrom, Phys. Rev. B 43, 12437 (1993-I).
54. A. J. Epstein, J. M. Ginder, F. Zuo, R. W. Bigelow, H.-S. Woo, D. B. Tanner, A. F. Richter, W.-S. Huang, and A. G. MacDiarmid, Synth. Met. 18, 303 (1987).
55. S. Stafstrom, J. L. Brédas, A. J. Epstein, H. S. Woo, D. B. Tanner, W. S. Huang, and A. G. MacDiarmid, Phys. Rev. Lett. 59, 1464 (1987).
56. J. L. Brédas, B. Thémans, J. G. Fripiat, J. M. André, and R. R. Chance, Phys. Rev. B 29, 6761 (1984).
57. T. Ohsawa, O. Kimura, M. Onoda, and K. Yoshino, Synth. Met. 47, 151 (1992).
58. M. Bartonek and H. Kuzmany, Synth. Met. 41-43, 607 (1991).
59. K. Mizoguchi, T. Obana, S. Ueno, and K. Kume, Synth. Met. 55-57, 601 (1993).
60. F. Genoud, M. Nechtschein, and C. Santier, Synth. Met. 55-57, 642 (1993).
61. J. M. Ginder, A. F. Richter, A. G. MacDiarmid, and A. J. Epstein, Solid State Commun. 63, 97 (1987).
62. M. E. Jozefowicz, R. Laversanne, H. H. S. Javadi, A. J. Epstein, J. P. Pouget, X. Tang, and A. G. MacDiarmid, Phys. Rev. B 39, 12958 (1989).
63. J. Tsukamoto, Adv. in Phys. 41, 509 (1992); J. Tsukamoto, A. Takahashi, and K. Kawasaki, Japan, J. Appl. Phys. 29, 125 (1990).
64. H. Naarmann and N. Theophilou, Synth. Met. 22, 1 (1987).
65. H. Shirakawa, Y.-X. Zhang, T. Okuda, K. Sakamaki, and K. Akagi, Synth. Met. 65, 93 (1994).
66. T. Ito, H. Shirakawa, and S. Ikeda, J. Polm. Sci. Polym. Chem. Ed. 12, 11 (1974).
67. K. Ito, Y. Tanabe, K. Akagi, and H. Shirakawa, Phys. Rev. B 45, 1246 (1992).
68. J. H. Edwards and W. J. Feast, Polymer Commun. 21, 595 (1980).
69. J. C. W. Chien, in *Polyacetylene: Chemistry, Physics, and Material Science* (Academic, New York, 1984), p. 24.
70. T. Ishiguro, H. Kaneko, Y. Nogami, H. Nishiyama, J. Tsukamoto, A. Takahashi, M. Yamaura, and J. Sato, Phys. Rev. Lett. 69, 660 (1992), H. Kaneko, T. Ishiguro, J. Tsukamoto, and A. Takahashi, Solid State Commun. 90, 83 (1994).
71. P. N. Adams, P. Laughlin, A. P. Monkman, and N. Bernhoeft, Solid State Commun. 91, 895 (1994); the value of conductivity reported in Fig. 4 is for samples kindly provided by Monkman and coworkers, and measured at The Ohio State University.
72. R. D. McCullough, S. P. Williams, S. Tristran-Nagle, M. Jayaraman, P. C. Ewbank, and L. Miller, Synth. Met. 69, 279 (1995).
73. J. Joo, Z. Oblakowski, G. Du, J. P. Pouget, E. J. Oh, J. M. Weisinger, Y. Min, A. G. MacDiarmid, and A. J. Epstein, Phys. Rev. B 49, 2977 (1994).
74. R. S. Kohlman, J. Joo, Y. Z. Wang, J. P. Pouget, H. Kaneko, T. Ishiguro, and A. J. Epstein, Phys. Rev. Lett. 74, 773 (1995).
75. A. J. Epstein, J. Joo, R. S. Kohlman, G. Du, A. G. MacDiarmid, E. J. Oh, Y. Min, J. Tsukamoto, H. Kaneko, and J. P. Pouget, Synth. Met. 65, 149 (1994).
76. A. J. Epstein, H. Rommelmann, M. A. Druy, A. J. Heeger, and A. G. MacDiarmid, Solid State Commun. 38, 683 (1981).
77. P. K. Kahol, H. Guan, and B. J. McCormick, Phys. Rev. B 44, 10393 (1991).
78. S. Ikehata, J. Kaufer, T. Woerner, A. Pron, M. A. Druy, A. Sivak, A. J. Heeger, and A. G. MacDiarmid, Phys. Rev. Lett. 45, 1123 (1980).
79. N. S. Sariciftı, A. J. Heeger, and Y. Cao, Phys. Rev. B 49, 5988 (1994).
80. (a) Y. W. Park, Synth. Met. 45, 173 (1991); (b) Y. W. Park, A. J. Heeger, M. A. Druy, and A. G. MacDiarmid, J. Chem. Phys. 73, 946 (1980).
81. H. H. S. Javadi, A. Chakraborty, C. Li, N. Theophilou, D. B. Swanson, A. G. MacDiarmid, and A. J. Epstein, Phys. Rev. B 43, 2183 (1991).
82. J. C. Clark, G. G. Ihas, A. J. Rafanello, M. W. Meisel, M. Reghu, C. O. Yoon, Y. Cao, and A. J. Heeger, Synth. Met. 69, 215 (1995); R. S. Kohlman, A. J. Epstein, G. G. Ihas, and A. G. MacDiarmid, to be published.
83. A. J. Epstein, H. Rommelmann, R. Bigelow, H. W. Gibson, D. M. Hoffman, and D. B. Tanner, Phys. Rev. Lett. 50, 1866 (1983).
84. Y. Cao, P. Smith, and A. J. Heeger, Synth. Met. 48, 91 (1992).
85. Y. Z. Wang, J. Joo, C.-H. Hsu, J. P. Pouget, and A. J. Epstein, Phys. Rev. B 50, 16811 (1994).
86. Z. H. Wang, H. H. S. Javadi, A. Ray, A. G. MacDiarmid, and A. J. Epstein, Phys. Rev. B 42, 5411 (1990).
87. J. Yue, Z. H. Wang, K. R. Cromack, A. J. Epstein, and A. G. MacDiarmid, J. Am. Chem. Soc. 113, 2655 (1991).
88. M. Yamaura, T. Hagiwara, and K. Iwata, Synth. Met. 26, 209 (1988).
89. K. Sato, M. Yamaura, T. Hagiwara, K. Murata, and M. Tokumoto, Synth. Met. 40, 35 (1991).
90. J.-E. Österholm, P. Passiniemi, H. Isotalo, and H. Stubb, Synth. Met. 18, 213 (1987).
91. T. Ohnishi, T. Noguchi, T. Nakano, M. Hirooka, and I. Murase, Synth. Met. 41–43, 309 (1991).
92. L. W. Shacklette, R. R. Chance, D. M. Ivory, G. G. Miller, and R. H. Baughman, Synth. Met. 1, 307 (1979).
93. G. Du, V. N. Prigodin, A. Burns, C. S. Wang, and A. J. Epstein, submitted.
94. A. J. Epstein, H. Rommelmann, M. Abkowitz, and H. W. Gibson, Phys. Rev. Lett. 47, 1549 (1981).
95. A. J. Epstein, H. Rommelmann, and H. W. Gibson, Phys. Rev. B 31, 2502 (1985).

96. F. Zuo, M. Angelopoulos, A. G. MacDiarmid, and A. J. Epstein, Phys. Rev. B **39**, 3570 (1989).
97. J. C. Scott, P. Pfluger, M. T. Krounbi, and G. B. Street, Phys. Rev. B **28**, 2140 (1983).
98. G. E. Wnek, J. C. Chien, F. E. Karasz, and C. P. Lillya, Polymer **20**, 1441 (1979).
99. R. E. Peierls, *Quantum Theory of Solid* (Clarendon, Oxford, 1955), p. 108.
100. E. J. Mele and M. J. Rice, Phys. Rev. B **23**, 5397 91981).
101. S. A. Kivelson and A. J. Heeger, Phys. Rev. Lett. **55**, 308 (1985).
102. H.-Y. Choi and E. J. Mele, Phys. Rev. B **34**, 8750 (1986).
103. D. B. Tanner, G. L. Doll, A. M. Rao, P. C. Eklund, G. A. Arbuckle, and A. G. MacDiarmid, Synth. Met. **28**, D141 (1989).
104. Y. H. Kim and A. J. Heeger, Phys. Rev. B **40**, 8393 (1989).
105. M. I. Salkola and S. A. Kivelson, Phys. Rev. B **50**, 13962 (1994); S. A. Kivelson and M. I. Salkola, Synth. Met. **44**, 281 (1991).
106. J. Tanaka, C. Tanaka, T. Miyamae, M. Shimizu, S. Hasegawa, K. Kamiya, and K. Seki, Synth. Met. **65**, 173 (1994).
107. A. Yamashiro, A. Ikawa, and H. Fukutome, Synth. Met. **65**, 233 (1994).
108. H. L. Wu and P. Phillips, Phys. Rev. Lett. **66**, 1366 (1991); P. Phillips and H. L. Wu, Science **252**, 1805 (1991).
109. F. C. Lavarda, M. C. dos Santos, D. S. Galvao, and B. Laks, Phys. Rev. Lett. **73**, 1267 (1994).
110. S. Stafstrom and J. L. Brédas, Phys. Rev. B **38**, 4180 (1988).
111. D. S. Galvao, D. A. dos Santos, B. Laks, C. P. de Melo, and M. J. Caldas, Phys. Rev. Lett. **63**, 786 (1989).
112. V. N. Prigodin and K. B. Efetov, Phys. Rev. Lett. **70**, 2932 (1993).
113. C. Kittel, in *Introduction to Solid State Physics* (John Wiley & Sons, Inc., New York, 1986), p. 157.
114. P. W. Anderson, Phys. Rev. **109**, 1492 (1958).
115. N. F. Mott and E. Davis, in *Electronic Processes in Non-Crystalline Materials* (Clarendon Press, Oxford, 1979), p. 6.
116. M. Reghu, C. O. Yoon, D. Moses, A. J. Heeger, and Y. Cao, Phys. Rev. B **48**, 17685 (1993); M. Reghu, Y. Cao, D. Moses, and A. J. Heeger, *ibid.* **47**, 1758 (1993).
117. C. O. Yoon, M. Reghu, D. Moses, A. J. Heeger, and Y. Cao, Phys. Rev. B **48**, 14080 (1993).
118. C. O. Yoon, M. Reghu, D. Moses, and A. J. Heeger, Phys. Rev. B **49**, 10851 (1994).
119. A. L. Efros and B. I. Shklovski, J. Phys. **C8**, L49 (1975); B. I. Shklovski and A. L. Efros, in *Electronic Properties of Doped Semiconductors* (Springer-Verlag, Heidelberg, 1984).
120. J. Joo, V. N. Prigodin, Y. G. Min, A. G. MacDiarmid, and A. J. Epstein, Phys. Rev. B **50**, 12226 (1994).
121. Z. H. Wang, A. Ray, A. G. MacDiarmid, and A. J. Epstein, Phys. Rev. B **43**, 4373 (1991).
122. S. Kivelson and A. J. Heeger, Synth. Met. **22**, 371 (1988).
123. P. Drüde, Ann. Phys. **1**, 566 (1900); **3**, 369 (1900).
124. G. Burns, in *Solid State Physics* (Academic, New York, 1985), p. 187.
125. R. H. Baughman, N. S. Murthy, and G. G. Miller, J. Chem. Phys. **79**, 515 (1983).
126. D. Chen, M. J. Winokur, M. A. Masse, and F. E. Karasz, Phys. Rev. B **41**, 6759 (1990).
127. J. P. Pouget, M. E. Jozefowicz, A. J. Epstein, X. Tang, and A. G. MacDiarmid, Macromolecules **24**, 779 (1991).
128. J. P. Pouget, C.-H. Hsu, A. G. MacDiarmid, and A. J. Epstein, Synth. Met. **69**, 119 (1995).
129. W. Fosong, T. Jinsong, W. Lixiang, Z. Hongfang, and M. Zhishen, Mol. Cryst. Liq. Cryst. **160**, 175 (1988).
130. Y. B. Moon, Y. Cao, P. Smith, and A. J. Heeger, Polym. Commun. **30**, 196 (1989).
131. M. E. Jozefowicz, A. J. Epstein, J. P. Pouget, J. G. Masters, A. Ray, and A. G. MacDiarmid, Macromolecules **25**, 5863 (1991).
132. J. Joo, Ph.D. Thesis, *Charge Localization and Delocalization Phenomena in Conducting Polymers*, The Ohio State University (1994); J. P. Pouget, to be published.
133. M. Laridjani, J. P. Pouget, E. M. Scherr, A. G. MacDiarmid, M. E. Jozefowicz, and A. J. Epstein, Macromolecules **25**, 4106 (1992).
134. A. G. MacDiarmid and A. J. Epstein, Synth. Met. **65**, 103 (1994).
135. A. G. MacDiarmid, J. M. Weisinger, and A. J. Epstein, Bull. Am. Phys. Soc. **38**, 311 (1993); A. G. MacDiarmid and A. J. Epstein, Trans. 2nd Congresso Brazileiro de Polimeros, São Paulo, Brazil, Oct. 5–8, 1993, p. 544; Y. Min, A. G. MacDiarmid, and A. J. Epstein, Polymer Preprints **35**, 231 (1994).
136. Y. Nagomi, J. P. Pouget, and T. Ishiguro, Synth. Met. **62**, 257 (1994).
137. P. A. Albouy, J. P. Pouget, J. Halim, V. Enkelmann, and G. Wegner, Makromol. Chem. **193**, 853 (1992); P. Robin, J. P. Pouget, R. Comes, H. W. Gibson, and A. J. Epstein, Polymer **24**, 1558 (1983).
138. P. Pfluger, M. T. Krounbi, and G. B. Street, Phys. Rev. B **28**, 2140 (1983).
139. J. Chen and A. J. Heeger, Synth. Met. **24**, 311 (1988).
140. N. Theophilou, D. B. Swanson, A. G. MacDiarmid, A. Chakraborty, H. H. S. Javadi, R. P. McCall, S. P. Treat, F. Zuo, and A. J. Epstein, Synth. Met. **28**, 35 (1988).
141. X. Q. Yang, D. B. Tanner, M. J. Rice, H. W. Gibson, A. Feldblum, and A. J. Epstein, Solid State Commun. **61**, 335 (1987).
142. Y. Nogami, H. Kaneko, T. Ishiguro, A. Fakahashi, J. Tsukamoto, and N. Hosoito, Solid State Commun. **76**, 583 (1990).
143. Z. H. Wang, C. Li, E. M. Scherr, A. G. MacDiarmid, and A. J. Epstein, Phys. Rev. Lett. **66**, 1749 (1991); Z. H. Wang, E. M. Scherr, A. G. MacDiarmid, and A. J. Epstein, Phys. Rev. B **45**, 4190 (1992).
144. Y. Cao and A. J. Heeger, Synth. Met. **52**, 193 (1992).
145. P. Pfluger, U. M. Gubler, and G. B. Street, Solid State Commun. **49**, 911 (1984).
146. K. Mizoguchi, K. Misoo, K. Kume, K. Kaneto, T. Shiraishi, and K. Yoshino, Synth. Met. **18**, 195 (1987).
147. K. Kume, K. Mizuno, K. Mizoguchi, K. Nomura, Y. Maniwa, J. Tanaka, M. Tanaka, and A. Watanabe, Mol. Cryst. Liq. Cryst. **83**, 285 (1982).
148. M. Onoda, Y. Manda, T. Iwasa, S. Morita, T. Kawai, and K. Yoshino, Synth. Met. **41–43**, 1349 (1991).
149. H. Kaneko and T. Ishiguro, Synth. Met. **65**, 141 (1994).
150. M. Reghu, K. Vakiparta, Y. Cao, and D. Moses, Phys. Rev. B **49**, 16162 (1994).
151. A. G. Zabrodskii and K. N. Zeninova, Zh. Eksp. Teor. Fiz. **86**, 727 (1984) [Sov. Phys. JETP **59**, 425 (1984)].
152. A. I. Larkin and D. E. Khmelnitskii, Zh. Eskp. Teor. Fiz. **83**, 1140 (1982) [Sov. Phys. JETP **56**, 647 (1982)].
153. P. Lee and T. V. Ramakrishnan, Rev. Mod. Phys. **57**, 287 (1985); H. Fukuyama, in *Electron-Electron Interactions in Disordered Systems*, edited by A. L. Efros and M. Pollak (Elsevier Science Publishers, New York, 1985), p. 155.
154. D. E. Khmelnitskii and A. I. Larkin, Solid State Commun. **39**, 1069 (1981).
155. Y. Nogami, H. Kaneko, H. Ito, T. Ishiguro, T. Sasaki, N. Toyota, A. Takahashi, and J. Tsukamoto, Phys. Rev. B. **43**, 11829 (1991).
156. F. Zuo, M. Angelopoulos, A. G. MacDiarmid, and A. J. Epstein, Phys. Rev. B **36**, 3475 (1987).
157. A. B. Kaiser, C. K. Subramaniam, P. W. Gilberd, and B. Wessling, Synth. Met. **69**, 197 (1985); R. Pelster, G. Nimtz, and B. Wessling, Phys. Rev. B **49**, 12718 (1994).
158. J. Joo, S. M. Long, J. P. Pouget, E. J. Oh, Y. Min, A. G. MacDiarmid, and A. J. Epstein, submitted.
159. H. Kaneko, T. Ishiguro, K. Sato, T. Hagiwara, M. Yamaura, H. Nishiyama, and H. Ishimoto, Synth. Met. **55–57**, 1102 (1993).
160. J. Joo, G. Du, A. J. Epstein, V. N. Prigodin, and J. Tsukamoto, Phys. Rev. B **52**, 8060 (1995).
161. C. R. Fincher, M. Ozaki, M. Tanaka, D. Peebles, L. Lauchlin, A. J. Heeger, and A. G. MacDiarmid, Phys. Rev. B **20**, 1589 (1979).
162. G. Leising, Phys. Rev. B **38**, 10313 (1988).
163. J. Tanaka and M. Tanaka, in *Handbook of Conducting Polymers*, edited by T. A. Skotheim (Marcel Dekkar, New York, 1986), p. 1269.
164. R. P. McCall, J. M. Ginder, J. M. Leng, H. J. Ye, S. K. Manohar, J. G. Masters, G. E. Asturias, A. G. MacDiarmid, and A. J. Epstein, Phys. Rev. B **41**, 5202 (1990).
165. J. M. Leng, R. P. McCall, K. R. Kromack, Y. Sun, S. K. Manohar, A. G. MacDiarmid, and A. J. Epstein, Phys. Rev. B **48**, 15719 (1993).
166. K. Yakushi, L. J. Lauchlan, T. C. Clarke, and G. B. Street, J. Chem. Phys. **79**, 4774 (1983).
167. G. B. Street, T. C. Clarke, M. Krounbi, K. K. Kanazawa, V. Y. Lee, P. Pfluger, J. C. Scott, and G. Weiser, Mol. Cryst. Liq. Cryst. **83**, 253 (1982); G. B. Street, T. C. Clarke, R. H. Geiss, V. Y. Lee, A. Nazzal, P. Pfluger, J. C. Scott, and G. Weiser, J. Phys. (Paris) **44**, C3–599 (1983).
168. S. Hotta, S. D. D. V. Rughooputh, A. J. Heeger, and F. Wudl, Macromolecules **20**, 212 (1987).
169. M. Kobayashi, J. Chen, T. C. Chung, F. Moraes, A. J. Heeger, and F. Wudl, Synth. Met. **9**, 77 (1984).

170. K. Kaneto, K. Yoshino, and Y. Inuishi, Sol. Stat. Commun. **46**, 389 (1983).
171. T.-C. Chung, J. H. Kaufman, A. J. Heeger, and F. Wudl, Phys. Rev. B. **30**, 702 (1984).
172. M. Satoh, M. Tabata, F. Uesugi, K. Kaneto, and K. Yoshino, Synth. Met. **17**, 595 (1987).
173. D. L. Gin, J. K. Avlyanov, and A. G. MacDiarmid, Synth. Met. **66**, 169 (1994).
174. L. M. Goldenberg and P. C. Lacaze, Synth. Met. **58**, 271 (1993).
175. N. F. Colaneri, D. D. C. Bradley, R. H. Friend, P. L. Burn, A. B. Holmes, and C. W. Spangler, Phys. Rev. B **42**, 11670 (1990).
176. J. D. Stenger Smith, R. W. Lenz, and G. Wegner, Polymer **30**, 1048 (1989).
177. R. H. Friend, D. D. C. Bradley, and P. Townsend, J. Phys. D: Appl. Phys. **20**, 1367 (1987).
178. D. D. C. Bradley, A. R. Brown, P. L. Burn, J. H. Burroughes, R. H. Friend, A. B. Holmes, K. D. Mackay, and R. N. Marks, Synth. Met. **41–43**, 3135 (1991).
179. K. Pichler, D. A. Halliday, D. D. C. Bradley, P. L. Burn, R. H. Friend, and A. B. Holmes, J. Phys. Condens. Matter **5**, 7155 (1993).
180. D. D. Gebler, Y. Z. Wang, J. W. Blatchford, S. W. Jessen, L. B. Lin, T. L. Gustafson, H. L. Wang, T. M. Swager, A. G. MacDiarmid, and A. J. Epstein, J. Appl. Phys. **78**, 4264 (1995).
181. S. W. Jessen, D. D. Gebler, Y. Z. Wang, J. W. Blatchford, L. B. Lin, T. L. Gustafson, H. L. Wang, T. M. Swager, A. G. MacDiarmid, and A. J. Epstein, Polym. Mat. Sci. Eng. **72**, 573 (1995).
182. M. Furukawa, K. Mizuno, A. Matsui, S. D. D. V. Ruhooputh, and W. C. Walker, J. Phys. Soc. Japan **58**, 2976 (1989).
183. U. Rauscher, H. Bässler, D. D. C. Bradley, and M. Hennecke, Phys. Rev. B **42**, 9830 (1990).
184. K. Pakbaz, C. H. Lee, A. J. Heeger, T. W. Hagler, and D. McBranch, Synth. Met. **64**, 295 (1994).
185. F. Wooten, in *Optical Properties of Solids* (Academic, New York, 1972), p. 173.
186. H. S. Woo, D. B. Tanner, N. Theophilou, and A. G. MacDiarmid, Synth. Met. **41–43**, 159 (1991).
187. S. Hasegawa, K. Kamiya, J. Tanaka, and M. Tanaka, Synth. Met. **14**, 97 (1986); J. Tanaka, S. Hasegawa, T. Miyamae, and M. Shimizu, Synth. Met. **41–43**, 1199 (1991).
188. T. Miyamae, M. Shimizu, and J. Tanaka, Bull. Chem. Soc. Jpn. **67**, 40253 (1994).
189. X. Q. Yang, D. B. Tanner, A. Feldblum, H. W. Gibson, M. J. Rice, and A. J. Epstein, Mol. Crys. Liq. Cryst. **117**, 267 (1985).
190. S. Hasegawa, K. Kamiya, J. Tanaka, and M. Tanaka, Synth. Met. **18**, 225 (1987).
191. R. P. McCall, E. M. Scherr, A. G. MacDiarmid, and A. J. Epstein, Phys. Rev. B **50**, 5094 (1994).
192. R. S. Kohlman (unpublished).
193. R. S. Kohlman, J. Joo, Y. G. Min, A. G. MacDiarmid, and A. J. Epstein (to be published).
194. K. Lee, A. J. Heeger, and Y. Cao, Phys. Rev. B **48**, 14884 (1993).
195. Y. Xia, A. G. MacDiarmid, and A. J. Epstein, Macromolecules **27**, 7212 (1994).
196. Y. Xia, J. M. Weisinger, A. G. MacDiarmid, and A. J. Epstein, Chem. Mater. **7**, 443 (1995).
197. R. S. Kohlman, Y. Min, A. G. MacDiarmid, and A. J. Epstein, Synth. Met. **69**, 211 (1995).
198. R. S. Kohlman, T. Ishiguro, H. Kaneko, and A. J. Epstein, Synth. Met. **69**, 325 (1995).
199. K. Lee, M. Reghu, E. L. Yuh, N. S. Sariciftı, and A. J. Heeger, Synth. Met. **68**, 287 (1995).
200. N. F. Mott and M. Kaveh, Adv. Phys. **34**, 329 (1985).
201. N. F. Mott, in *Localization and Interaction in Disordered Metals and Doped Semiconductors*, edited by D. M. Finlayson, Proceedings of the Thirty-First Scottish Universities Summer School in Physics of 1986 (Scottish Universities Summer School in Physics, 1986).
202. N. F. Mott, in *Localization 1990*, edited by K. A. Benedict and J. T. Chalker (Inst. of Phys. Conf. Ser. No. 108, Institute of Physics, Bristol, Philadelphia, New York, 1990). Paper presented at the Localization 1990 Conference held at the Imperial College, London.
203. D. J. Bergman and D. Stroud, in *Solid State Physics*, edited by H. Ehrenreich and D. Turnbull (Academic, New York, 1992), vol. 46, p. 148.
204. *Intrinsically Conducting Polymers: An Emerging Technology*, edited by M. Aldissi (Kluwer Academic Publishers, Boston, 1993), *Science and Applications of Conducting Polymers*, edited by W. R. Salaneck and D. T. Clark (IOP Publishing, Lofthus, Norway, 1990).
205. A. G. MacDiarmid and R. B. Kaner, in *Handbook of Conducting Polymers*, edited by T. A. Skotheim (New York, Marcel Dekker, 1986), Vol. 1, p. 687; D. Naegele and R. Bittihn, Solid State Ionics **28–30**, 983 (1988); M. Maxfield, T. R. Jow, M. G. Sewchok, and L. W. Shacklette, J. of Power Sources **26**, 93 (1989).
206. N. F. Colaneri and L. W. Shacklette, IEEE Trans. Instru. Meas. **IM-41**, 291 (1992); T. Taka, Synth. Met. **41-43**, 1177 (1991).
207. J. Joo and A. J. Epstein, Appl. Phys. Lett. **65**, 2278 (1994).
208. T. Taka, Synth. Met. **41-43**, 1177 (1991).
209. J. Joo, A. G. MacDiarmid, and A. J. Epstein, Proc. Annual Technical Conf. of Plastic Engineers **2**, 1672 (1995).
210. A. J. Epstein, J. Joo, C. Y. Wu, A. Benatar, C. F. Faissi, Jr., J. Zegarski, and A. G. MacDiarmid, in *Intrinsically Conducting Polymers: An Emerging Technology*, edited by M. Aldissi (Kluwer Academic Publishers, Dordrecht, 1993), p. 165.
211. J. H. Burroughes, D. D. C. Bradley, A. R. Brown, R. N. Marks, K. Mackay, R. H. Friend, P. L. Burns, and A. B. Holmes, Nature **347**, 539 (1990); D. Braun and A. J. Heeger, Appl. Phys. Lett. **58**, 1982 (1991); P. L. Burns, A. B. Holmes, A. Kraft, D. D. C. Bradley, A. R. Brown, R. H. Friend, and R. W. Gymer, Nature **357**, 47 (1992); D. D. C. Bradley, Synth. Met. **54**, 401 (1993); I. D. Parker, J. Appl. Phys. **75**, 1656 (1994).
212. J. Yue and A. J. Epstein, J. Chem. Soc., Chem. Commun. **21**, 1540 (1992); F. Selampinar, L. Toppare, U. Akbulut, T. Yalcin, and S. Suzer, Synth. Met. **68**, 109 (1995); and references therein.
213. S. Jasty and A. J. Epstein, Polym. Mat. Sci. Eng. **72**, 565 (1995); D. W. DeBerry, J. Electrochem. Soc. **132**, 1022 (1985); N. Ahmad and A. G. MacDiarmid, Bull. Am. Phys. Soc. **32**, 548 (1987); B. Wessling, Adv. Mater. **6**, 226 (1994); W. K. Lu, R. L. Elsenbaumer, and B. Wessling, Synth. Met. **71**, 2163 (1995).
214. G. Gustafsson, Y. Cao, G. M. Treacy, F. Klavetter, N. Colaneri, and A. J. Heeger, Nature **357**, 477 (1992).
215. Y. Z. Wang, D. D. Gebler, L. B. Lin, J. W. Blatchford, S. W. Jessen, H. L. Wang, and A. J. Epstein, Appl. Phys. Lett. **68** (1996).
216. Y. Yang and A. J. Heeger, Appl. Phys. Lett. **64**, 1245 (1994); Y. Cao, G. M. Treacy, P. Smith, and A. J. Heeger, Appl. Phys. Lett. **60**, 2711 (1992).
217. A. Fizazi, J. Moulton, K. Pakbaz, S. D. D. V. Rughooputh, P. Smith, and A. J. Heeger, Phys. Rev. Lett. **64**, 2180 (1990).
218. C. O. Yoon, M. Reghu, D. Moses, A. J. Heeger, and Y. Cao, Synth. Met. **63**, 47 (1994).
219. G. Du, V. Prigodin, J. Avlyanov, A. G. MacDiarmid, and A. J. Epstein (to be published)